

Evaluation of mobile laser scanning acquisition scenarios for automated wood volume estimation in a temperate hardwood forest using quantitative structural models

Bastien Vandendaele ^{a,b}, Olivier Martin-Ducup ^c, Richard A. Fournier^b, and Gaetan Pelletier^a

^aNorthern Hardwoods Research Institute Inc., 165 boulevard Hébert, Edmundston, NB E3V 2S8, Canada; ^bDepartment of Applied Geomatics, Centre d'Applications et de Recherches en Télédétection (CARTEL), Université de Sherbrooke, 2500, Boul. de l'Université, Sherbrooke, QC J1K 2R1, Canada; ^cEcologies des Forêts Méditerranéennes (URFM), INRA, Avignon 84000, France

Corresponding author: Bastien Vandendaele (email: bastien.vandendaele@hardwoodsnb.ca)

Abstract

This study explores how data from a handheld mobile laser scanning (MLS) system and quantitative structural models (QSM) can be used to estimate tree structural attributes. Four MLS acquisition scenarios were investigated in a 1 ha temperate hardwood stand, including 15 and 35 m parallel lines, nine circular plots, and a 20 m × 20 m grid. Results were compared against terrestrial laser scanning and destructive field measurements. All acquisition scenarios yielded comparable results, except for the 35 m scenario, which showed greater variability. The 20 m × 20 m grid scenario showed the highest accuracy, with an RMSE of 0.41 m (2.07%) for tree height, 3.98 cm (14.93%) for diameter at breast height, 0.21 m³ (19.28%) for merchantable wood volume, and 0.07 m³ (10.11%) for merchantable stem volume. A bias < 5% was observed for these key attributes, except for an 11.68% bias in merchantable wood volume. Overestimation of branch volume was identified as the primary source of bias related to merchantable wood volume. This study highlights MLS's potential for accurate, non-destructive estimation of tree structural attributes, while pointing out the need to refine noise removal and to assess the most suitable acquisition scenarios for various forest types.

Key words: mobile laser scanning, SLAM, tree attributes, quantitative structure model (QSM), volume

Résumé

Cette étude explore l'utilisation de données issues d'un lidar mobile (MLS) portatif et de modèles quantitatifs de structure (QSM) pour l'estimation des attributs structuraux des arbres. Quatre scénarios d'acquisition MLS ont été investigués dans une parcelle de forêt feuillue tempérée de 1-ha, incluant des trajectoires parallèles de 15 m et 35 m, neuf parcelles circulaires et une grille de 20 m × 20 m. Les résultats ont été comparés à ceux d'un lidar terrestre et de mesures destructives. Tous les scénarios d'acquisition ont produit des résultats comparables, à l'exception du scénario de 35 m, qui a montré une plus grande variabilité. Le scénario de la grille de 20 m × 20 m a montré la plus haute précision, avec un RMSE de 0.41 m (2.07%) pour la hauteur des arbres, 3.98 cm (14.93%) pour le diamètre à hauteur de poitrine, 0.21 m³ (19.28%) pour le volume de bois marchand et 0,07 m³ (10.11%) pour le volume de tige marchande. Un biais < 5% a été estimé pour ces attributs clés, à l'exception d'un biais de 11.68% pour le volume de bois marchand. La surestimation du volume des branches a été identifié comme la principale source de biais liée au volume de bois marchand. Cette étude met en évidence le potentiel du MLS pour l'estimation précise et non destructive des attributs structuraux des arbres. Elle souligne toutefois la nécessité d'affiner la réduction du bruit dans les données MLS et d'identifier les scénarios d'acquisition les plus appropriés pour différents types de forêts. [Ceci est une traduction fournie par l'auteur du résumé en anglais.]

Mots-clés : lidar mobile, SLAM, attributs forestiers, Modèles Quantitatifs de Structure (QSM), volume

1. Introduction

Accurate estimation of tree volume or aboveground biomass (AGB) is crucial for calibrating and validating biomass mapping products using Earth observation data (Duncanson et al. 2019). To determine AGB using satellite data, field measurements are required and traditionally ob-

tained by measuring tree attributes, including stem diameter at breast height (DBH), height, wood density, and species. These measurements are then converted to AGB values using allometric models (Demol et al. 2022a). Applying allometric models presents several challenges, primarily due to uncertainties in model selection (Duncanson et al. 2017). The cur-

rent approach to calibrating these models also involves destructive harvesting of trees, which is costly, invasive, and not always ethically or legally feasible. Consequently, allometric models often rely upon limited calibration data, thereby raising concerns about their spatial representation and applicability to different tree sizes (Chave et al. 2014; Aguilar et al. 2019). Thus, there is a pressing need to develop novel methods that are faster and more accurate, and which enable non-destructive calibration of allometric models (Duncanson et al. 2021).

Terrestrial laser scanning (TLS) is increasingly being recognized as a valuable alternative to field measurements for biomass estimates and is commonly employed as a ground truth validation method (Momo Takoudjou et al. 2018; Brede et al. 2019). Reconstruction techniques such as voxel-based methods (Bienert et al. 2014) or quantitative structural models (QSMs) (Raumonen et al. 2013; Hackenberg et al. 2015) are used to estimate the volume of each tree, which can be converted into an estimate of AGB using basic wood density (Demol et al. 2022a). Validation studies have extensively compared TLS-based tree volume or AGB estimates that are derived from QSMs with destructively measured values (e.g., Kunz et al. 2017; Brede et al. 2019; Burt et al. 2021; Fan et al. 2022). Calders et al. (2015) employed the TreeQSM algorithm (Raumonen et al. 2013) to estimate AGB of 65 eucalyptus trees (*Eucalyptus leucoxylon*, *E. microcarpa*, *E. tricarpa*) using TLS, resulting in 9.68% overestimation when compared to destructive measurements. Momo Takoudjou et al. (2018) assessed the accuracy of TLS for estimating volumes and AGB of large tropical trees in eastern Cameroon. They found that TLS-derived volumes using QSMs were highly reliable, with overall root-mean square error (RMSE) < 2.81%; coefficients were statistically comparable to destructive data for calibrating biomass allometric models. In a recent study by Demol et al. (2022a), a comprehensive global dataset of 391 trees from diverse forest conditions was analyzed using TLS scans and destructive measurements. The results demonstrated close agreement between TLS-derived AGB and destructive values, with bias < 1% and a concordance correlation coefficient of 98% (CCC, Lin 1989). Most notably, TLS estimates of AGB were less biased and more accurate compared to allometric models, thereby highlighting the effectiveness of the TLS-derived QSM approach. Yet, it is important to consider that the level of accuracy achieved can be substantially influenced by the complexity of the forest structure and the degree of manual fine-tuning in data processing. For instance, in undisturbed tropical forests, Martin-Ducup et al. (2021) reported that fully automated methods could result in relative volume errors ranging from 39% to 115% at the individual tree level. Yet, the incorporation of manual assistance, particularly in tasks such as tree segmentation, reduced the error on volume estimates by a factor of 10. This underscores the variability in TLS accuracy, depending upon forest type and the balance between automation and manual correction.

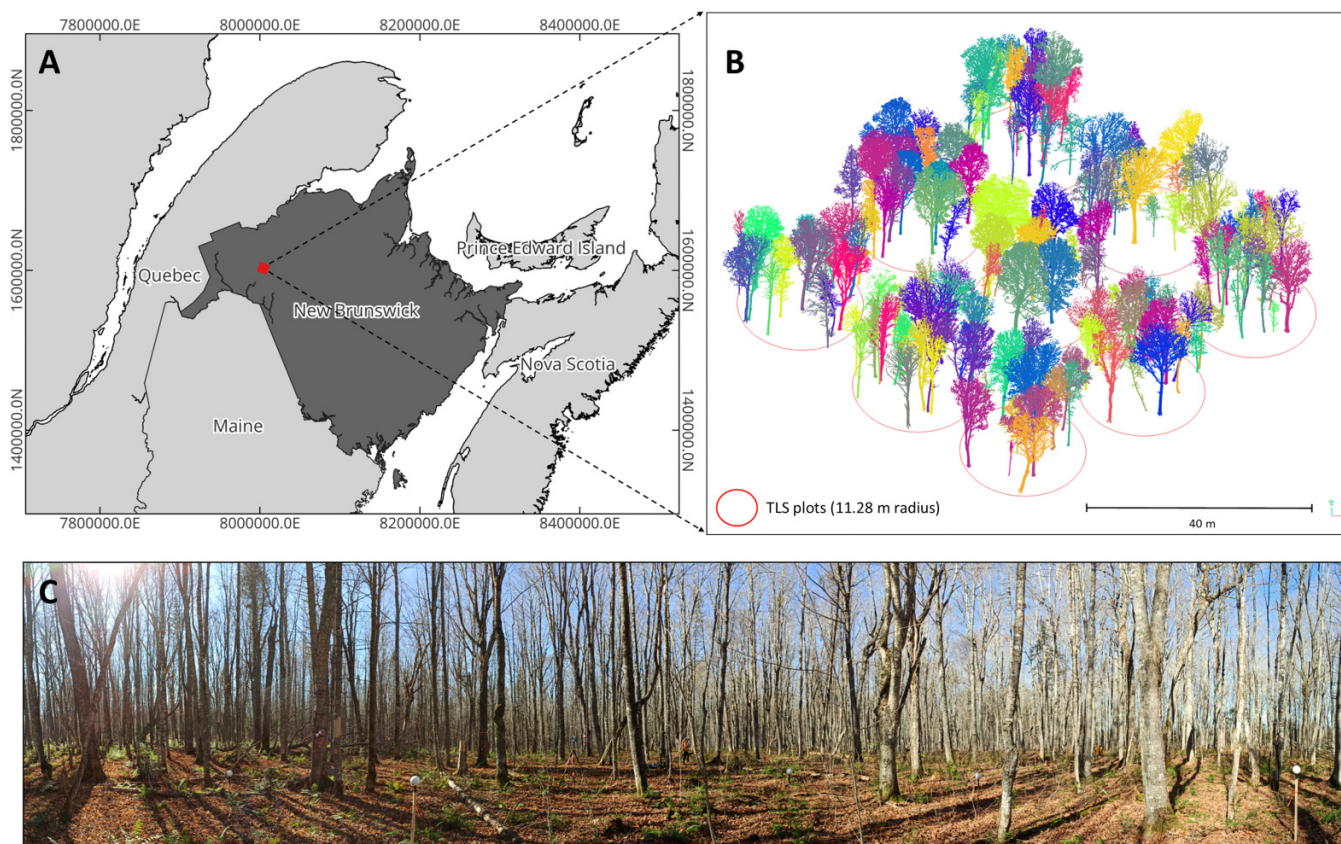
Despite the proven benefits of TLS-based QSM approaches for forest inventory, TLS itself has certain limitations, such as the need for multiple scanning stations, together with labour-intensive and time-consuming data acquisition processes. Occlusion that is caused by trees and understory vege-

tation also can pose challenges during data collection. These limitations have prompted researchers to seek a scalable technology that is capable of providing efficient and readily usable 3 D point clouds, with a benefit–cost ratio comparable to that of conventional manual measurements. Mobile laser scanning (MLS) has emerged as a promising alternative to TLS for forest inventories (Balenović et al. 2020; Gollob et al. 2020). MLS systems consist of a laser scanner that is either mounted on a vehicle or just carried by hand, which can rapidly scan the forest environment while moving along a designated path. MLS technology offers substantial advantages over traditional forest inventory methods or TLS, enabling efficient and cost-effective data collection while minimizing occlusion. Numerous studies have showcased the efficacy of MLS data in estimating various tree structural attributes, such as DBH (Gollob et al. 2020), height (Jurjević et al. 2020), stem taper (Hyyppä et al. 2020; Stovall et al. 2023) and merchantable volume (Vandendaele et al. 2022).

Despite these significant advancements, the application of MLS technology in forest inventory encounters three notable challenges. First, MLS data often contain substantial amounts of noise (Bauwens et al. 2016) and exhibit lower spatial accuracy due to propagation of positioning errors (Chen et al. 2019). Consequently, accurately extracting individual tree attributes becomes a challenging task. Second, the selection of appropriate sampling designs and data analysis methods has yet to be tested in forest inventory. Indeed, only a limited number of studies have investigated the influence of acquisition scenarios on tree attribute accuracy (Perugia et al. 2019; Mokoš et al. 2021; Kuželka et al. 2022; Tupinambá-Simões et al. 2023). Last, the lack of automated approaches for efficient processing of 3 D point clouds and production of useful outputs for foresters remains a substantial challenge (Martin-Ducup et al. 2021). Reliance upon manual steps and extensive expertise that is required in 3 D processing hampers the widespread adoption of this new technology in the field of forestry. Addressing these challenges through further research and technological advancements would unlock the full potential of MLS in compiling precision forest inventories.

In a previous study, we explored the potential of MLS data for extracting stem and merchantable wood volume in a northern hardwood stand, and comparing these estimates with TLS and destructive field samples (Vandendaele et al. 2022). Yet, this study was limited in scope, given that it involved only a small number of trees ($n = 26$). The methodology that was employed required heavy manual procedures for segmenting individual trees, with little emphasis on the influence posed by acquisition scenarios on the accuracy of tree attribute estimation. Building upon this foundation, the present paper takes a more comprehensive approach to dealing with the three aforementioned challenges. Therefore, we investigated four MLS acquisition scenarios over a 1-ha hardwood stand and employed a fully automated approach utilizing automatic tree segmentation and filtering, together with QSM for extracting key inventory attributes and merchantable wood volume. This study aims to achieve two objectives: (i) to assess the accuracy of MLS-based automated approaches in estimating individual tree volume through 3 D re-

Fig. 1. (A) Location of the study area. (B) Study site with the 9 terrestrial laser scanning (TLS) sample plots (11.28 m radius) and the 163 sample trees. (C) Panoramic view from one of the sample plots (photograph by Bastien Vandendaele ©). Figures were created using QGIS version 3.34.3 and assembled from publicly available data: state boundaries from GeoNB (<https://geonb.snb.ca/geonb/>), the 2016 Census Boundary Files (www.statcan.gc.ca), and the U.S. Census Bureau (<https://www.census.gov/geographies/mapping-files.html>).



construction, with comparisons to TLS and destructive measurements; and (ii) to compare different acquisition scenarios for tree attribute estimation using MLS data collection. This study offers valuable insights into the accuracy and efficiency of MLS-based forest inventory estimation. It also introduces an efficient and non-destructive method for automated processing of ground-based lidar point clouds, further enhancing the overall workflow of forest inventory analysis.

2. Materials and methods

2.1. Study site

The study site is located in Jardine Brook, southwest of Saint-Quentin (NB, Canada), on a 1 ha mature hardwood site at 280 m a.s.l. (47°25'21.70"N, 67°31'5.84"W) (Fig. 1). This site is part of the Central Uplands Ecoregion of Madawaska in the temperate hardwood zone (Zelazny et al. 2007). The study site is on flat terrain (slope < 1%), with a crown closure of 56%, little understory or shrub presence. Trees in the 1 ha hardwood stand have a mean height of 18 m (SD ± 5.6 m) and mean crown base height of 7.6 m (SD ± 2.9 m). The stand has not been subjected to high-intensity treatments since the early 1940s, except for very light removals (<10% basal

area) to salvage balsam fir mortality. There are about 500 merchantable stems per hectare in the stand, with a basal area of 16 m²·ha⁻¹. The stand is multi-age, having more than two distinct cohorts or age classes (from 75- to 160-years old) and is composed mainly of sugar maple (*Acer saccharum* Marshall, 88% basal area), yellow birch (*Betula alleghaniensis* Britton, 10%), and balsam fir (*Abies balsamea* [L.] Miller, 2%).

2.2. Terrestrial laser scanning (TLS) and field inventory data

The TLS data were acquired during leaf-off conditions in October 2021 using a FARO Focus3D S 120 scanner (Faro Technologies Inc., Lake Mary, FL, USA). Nine sample plots of 11.28 m radius (400 m² with a 10 m buffer) were scanned within the 1 ha study site (Fig. 1). The scans were performed from five locations, including the plot centre and the four cardinal points of the plot, to minimize laser signal occlusion. The TopCon FC-500 Hiper SR Kit Rover (Tokyo, Japan) was used to measure the centre-point of each TLS plot. The location of three trees per sample plot and these centre-point locations were utilized as references for geo-referencing the TLS point cloud and co-registering the scans with the MLS data. TLS has a beam divergence of 0.27 mrad (0.015°), resulting in a laser beam footprint of 2.62 mm in diameter

Table 1. Descriptive statistics of tree structural attributes for terrestrial laser scanning (TLS) reference trees within the 1 ha study site.

Attribute	Name	Range	Mean	Standard deviation
Number of TLS reference trees	<i>n</i>	163	<i>na</i>	<i>na</i>
Tree height (m)	H	7.48–24.8	19.8	4.71
Diameter at breast height (cm)	DBH	5.69–64.66	26.71	12.45
Crown projected area (m ²)	CPA	0.37–86.48	22.63	18.8
Alpha volume (m ³)	AV	0.58–589.15	119.53	120.46
Total volume (m ³)	<i>V</i> _{tot}	0.05–4.68	1.26	1.02
Merchantable volume (m ³)	<i>V</i> _{merch}	0.02–3.67	0.98	0.83
Operational merchantable volume (m ³)	<i>V</i> _{op}	0.02–3.55	0.95	0.80
Merchantable stem volume (m ³)	<i>V</i> _{stem}	0.02–2.59	0.77	0.56

Note: A detailed description of each tree structural attribute is provided in Table 2 (Section 2.4.3). na, not applicable.

at a distance of 10 m from the sensor. It was parameterized to achieve a point spacing of 6.3 mm at this distance. Eight spherical targets were positioned within each sample plot to enable co-registration of multiple scans using FARO SCENE 5.1.6.3 software. The scan co-registration process had a mean absolute error of 6.0 mm.

A total of 163 trees from the nine TLS sample plots (Fig. 1 and Table 1) were identified through semi-automatic TLS segmentation (Section 2.4.1). They composed the benchmark dataset against which MLS-derived attributes were compared. The validation dataset excluded broken trees, dead trees, or severely occluded trees in the point cloud. From the 163 TLS reference trees, 26 (~3 trees per plot) were harvested and processed in March 2022 following the procedure detailed in Vandendaele et al. (2022). Each felled tree was cut into bucked segments for all stem or branches of significant size. All branches with the smallest piece being ≥ 244 cm long and with a small end diameter outside bark (DOB) ≥ 8 cm were measured. Manual measurements included stump height, segment lengths, and widest and narrowest DOBs at both ends of the segments. These were then applied to the Smalian formula (Bruce and Schumacher 1950) to estimate the operational merchantable volume of a tree (see Section 2.4.3 for wood volume nomenclature). In addition, the merchantable stem volume was calculated using the Li and Weiskittel (2012) taper model (Li et al. 2012; Weiskittel and Li 2012), which uses tree height and DBH as predictors and is specifically tailored for hardwood species in the Acadian region. These calculated volumes provided benchmarks for validating MLS data estimates, reflecting traditional volume assessment methods in New Brunswick forestry.

2.3. Mobile laser scanning (MLS) data

The MLS data were collected during leaf-off condition in October 2021 using the Hovermap (Emesent Pty Ltd, Milton, QLD, Australia), which is a handheld device that includes a Velodyne (Velodyne Lidar Inc., Morgan Hill, CA, USA) VLP-16 Lite lidar, a data logger, and an inertial measurement unit (IMU). The lidar has 16 channels and can capture up to 600 000 points s^{-1} , with a maximum range of 100 m and beam divergence of 3 mrad (0.17°). This results in a laser beam footprint of 29.67 mm in diameter at a distance of 10 m.

The system records distances with a continuous wavelength of 903 nm and a lidar accuracy of ± 3 cm. The Hovermap uses simultaneous localization and mapping (SLAM) technology to generate a 3 D point cloud without requiring artificial reference targets or tripods. It uses lidar and IMU data for real-time mapping and generates a coherent map of its surroundings. Loop closure, or using the same point for start and finish, is recommended to update real-time mapping and reduce potential drifts that are associated with the SLAM algorithm.

Four MLS acquisition scenarios were investigated to scan the 1 ha study site (Fig. 2). The first scenario, which is referred to as MLS_{15m}, followed a parallel line trajectory at 15 m intervals in a ~30 min walk, achieving an average point density of 15.6 k points·m⁻². The second scenario, MLS_{35m}, also followed a parallel line pattern but at wider 35 m intervals during a shorter ~15 min walk, resulting in an average point density of 7.3 k points·m⁻². The third scenario, referred to as MLS_{9plots}, consisted of scanning nine circular plots following a flower petal pattern in a ~35 min walk, each plot encircled by a concentric circle, achieving an average point density of 17.1 k points·m⁻². The fourth scenario, MLS_{grid20m}, involved walking along a 20 m \times 20 m grid pattern for ~40 min, periodically returning to the centre at each corner of the site, with an average point density of 16.8 k points·m⁻². Hovermap data underwent automated pre-processing using Emesent 1.5.0 proprietary software (Milton, QLD).

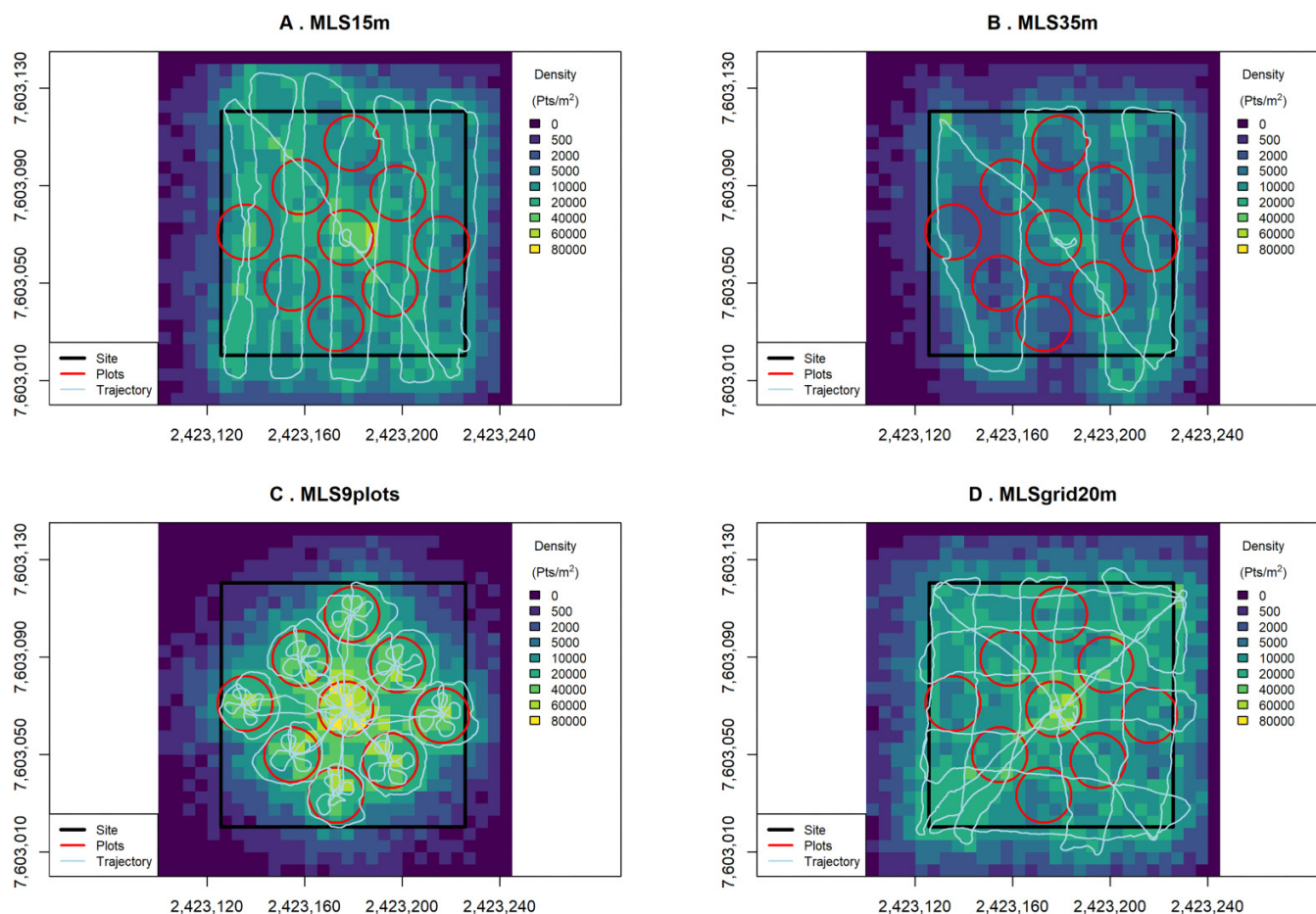
2.4. Methods

The overall data processing workflow for MLS data (Fig. 3) shows the main steps that were performed to estimate tree attributes. These steps include (i) lidar data acquisition and pre-processing, (ii) automatic segmentation of individual trees, (iii) tree cleaning and filtering, (iv) tree structural attributes estimation and wood volume estimation through QSM, and (v) validation of the estimated attributes.

2.4.1. Segmentation of individual trees

The geo-referenced TLS sample plots and the four MLS acquisitions were first co-registered in CloudCompare (CloudCompare Version 2.11.3) using the fine registration It-

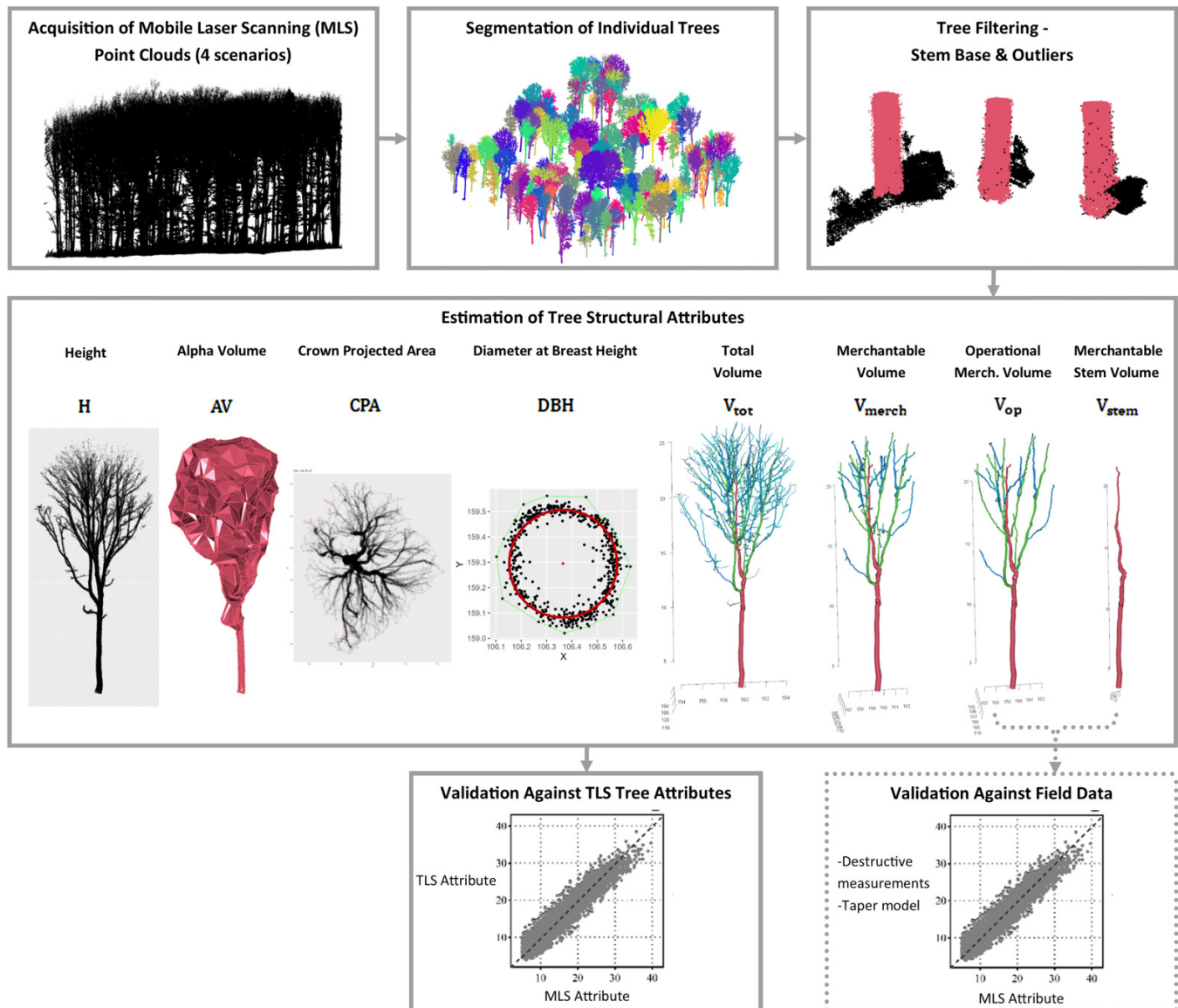
Fig. 2. Representative point density from mobile laser scanning (MLS) across different acquisition scenarios over the 1 ha hardwood site with a 20 m buffered area: (A) MLS_{15m} : 15 m parallel lines (~30 min), (B) MLS_{35m} : 35 m parallel lines (~15 min), (C) MLS_{9plots} : 9 circular plots (~35 min), and (D) $MLS_{grid20m}$: 20 m \times 20 m grid (~40 min). Voxelization was performed with a resolution of 1 cm. The colour gradient indicates the point density (Pts. m^{-2}) at a 5 m pixel resolution, ranging from low (purple) to high (yellow). The black outlines delimit the study site boundary, while the red outlines indicate the location of the nine terrestrial laser scanning (TLS) sample plots. Turquoise lines represent the trajectory of the MLS data acquisition scenario.



erative Closest Point (ICP) algorithm. Each TLS and MLS sample plot was extracted based on its geo-location, with a 10 m buffer extending the plot area and downsampled at 1 cm using a voxel grid filter. This process ensured a uniform point distribution, facilitating the effective application of clustering algorithms (Raumonen et al. 2013). The SimpleTree algorithm (Hackenberg et al. 2015) from the Computree platform (Othmani et al. 2011) was used to segment individual trees with a height ≥ 6 m from the sample plots. This algorithm takes a bottom-up approach, first identifying the stem and then using it as a seed to delineate the tree from its neighbours. The “filter cluster by the distance of the bounding box to a given point” function from the SimpleTree toolbox (Hackenberg et al. 2015) was used to extract trees located within a 12 m radius from the centre of each plot. While both the TLS and MLS data were segmented automatically, the results of the TLS individual tree segmentation were refined manually in CloudCompare to eliminate any anomalies in the reference dataset.

An algorithm was developed in R (R Core Team 2017) to match pairs of TLS and MLS trees by considering their geo-location and the percentage of non-empty voxels overlapping. It comprises three sequential steps: (i) voxelization of the point cloud at 0.5 m; (ii) calculation of the percentage of non-empty voxels overlapping between the point clouds; and (iii) selection of the point cloud(s) with a voxel overlap $> 50\%$ as a potential match. Multiple matches are possible, but they are highly unlikely. In such cases, the tree with the greatest voxel overlap is selected as the match. From the 163 TLS reference trees, the automated matching process yielded a total match of 156 trees for the MLS_{15m} scenario (95.7%), 154 for MLS_{35m} (95.5%), 155 for MLS_{9plots} (95.1%), and 157 for the $MLS_{grid20m}$ (96.3%). Minor variations in tree counts between MLS and TLS datasets are attributed to the border effect of the circular plot design and the automated spatial filtering method used. These discrepancies arise from shifts in tree bounding box centers caused by slight segmentation differences, leading to the occasional exclusion of

Fig. 3. Summary of the workflow performed in this research using mobile laser scanning (MLS) to estimate tree attributes and validate them against terrestrial laser scanning (TLS) and a sample of field data.



trees at the plot's edge during the automated spatial filtering step.

2.4.2. Tree filtering

The estimation of tree structural attributes and the application of QSMs requires well-segmented trees. However, some MLS trees that were segmented by SimpleTree algorithm may have low vegetation around the trunk base (Fig. 3). To address this issue, an R algorithm was developed to automatically clean the base of the trunk (below 1.5 m) by removing noise and low vegetation points. The algorithm applies the four following steps to the point cloud: (i) removal of points that are too far from the vertical using the geometrical point cloud feature that was proposed by Hackel et al. (2016), with a verticality threshold of 0.8; (ii) grouping the remaining points to distinguish trunk points and to remove surrounding noise;

(iii) removal of small groups of points to exclude outliers; and (iv) identifying the largest cluster of points as the trunk base. By using this algorithm, the base of the trunk was cleaned (Fig. 3) and the resulting QSM analysis was deemed to be more accurate. Each tree also was filtered using a statistical outlier removal (SOR) filter that is available in the VoxR package (Lecigne et al. 2018; Lecigne 2022; default parameters were used).

2.4.3. Estimation of tree structural attributes

Tree height (H), DBH, crown projected area (CPA) and alpha volume (AV) were estimated from the TLS and MLS segmented trees using ITSM R package (Terryn et al. 2023), as described in Table 2.

QSMs were computed for each TLS and MLS trees using TreeQSM algorithm (described by Raumonen et al. 2013;

Table 2. List of tree structural attributes, description, and algorithm used (see Fig. 3 for illustration).

Attribute	Name	Origin	Description	Algorithm
Height (m)	H	Point Cloud	Difference between the z-value of the highest and lowest point of the tree in the point cloud	R package: ITSMe (Terryn et al. 2023)
Diameter at breast height (cm)	DBH	Point Cloud	Diameter of a circle fitted through a 6 cm thick horizontal slice around 1.3 m using a least-squares circle-fitting algorithm	
Crown projected area (m ²)	CPA	Point Cloud	Area of the concave hull (concavity = 2) computed from the point cloud	
Alpha volume (m ³)	AV	Point Cloud	Volume of the 3 D alpha-shape computed from the point cloud using the alphashape3d R package (alpha = 1) (Lafarge & Pateiro-Lopez 2023)	
Total volume (m ³)	V _{tot}	QSM	Volume encompassing the stem (i.e., branching order 0) plus the volume of branches up to the third branching order (1–3)	TreeQSM (Raumonen and Åkerblom 2019) & R package: aRchi (Martin-Ducup and Lecigne 2022)
Merchantable volume (m ³)	V _{merch}	QSM	V _{tot} truncated to include only parts with a minimum diameter outside bark (DOB) at the wood segment small end of ≥ 8 cm	
Operational merchantable volume (m ³)	V _{op}	QSM	V _{tot} truncated to include only parts with a minimum DOB at the wood segment small end of ≥ 8 cm with the smallest branch pieces being ≥ 244 cm long. This volume is compatible with the way operational merchantable wood volume is measured in the field	
Merchantable stem volume (m ³)	V _{stem}	QSM	Volume of the stem (i.e., branching order 0) with a minimum DOB at the wood segment small end of ≥ 8 cm	

Note: Tree structural attributes derived from MLS data are denoted with the subscript “MLS”, and those derived from TLS data with “TLS”. MLS, mobile laser scanning; TLS, terrestrial laser scanning; QSM, quantitative structural models.

Åkerblom et al. 2015; Calders et al. 2015; Lecigne et al. 2018) version 2.3.3 in MATLAB (MATLAB 2023). The algorithm’s workflow, which is described in the TreeQSM 2.3.3 manual (Raumonen and Åkerblom 2019), was followed, including the use of its parallel computing capabilities. The approach that is described in Martin-Ducup et al. (2021) and in Vandendaele et al. (2022) was used to optimize model parameters and to select the best reconstruction. The optimization process enabled the generation of 32 QSM reconstructions per tree, utilizing varying parameter sets, as specified in the supplementary material of Martin-Ducup et al. (2021). The “select_optimum” function within TreeQSM, which prioritizes the minimal point-to-surface distance for stem and branches, was employed to select the most accurate reconstruction from the point cloud data. Given the stochastic nature of point clustering within the TreeQSM workflow, identical parameter inputs can result in slight variations in the generated QSMs (Calders et al. 2015). To account for this variability and ensure robust volume estimations, three QSMs were generated for every tree using the determined set of optimal parameters. The QSM that yielded the optimal fit based upon the “select_optimum” function was selected for wood volume estimation.

Total volume (V_{tot}), merchantable volume (V_{merch}), operational merchantable volume (V_{op}), and merchantable stem volume (V_{stem}), were derived from the QSMs using the aRchi R package (Martin-Ducup and Lecigne 2022), following the

methodology and nomenclature system that were detailed in Vandendaele et al. (2022). These four types of volume, described in Table 2 and illustrated in Fig. 3, were generated from all matched merchantable tree pairs (i.e., DBH ≥ 8 cm) that were identified in the nine sample plots from both MLS and TLS datasets (i.e., ~130 trees per scenario among the 163 trees). Furthermore, for a subset of 26 trees, field destructive volume measurements (Vandendaele et al. 2022, Section 2.2) were compared with V_{op_MLS}, with the MLS trees truncated at the stump height measured in the field for each tree.

2.4.4. Accuracy assessment

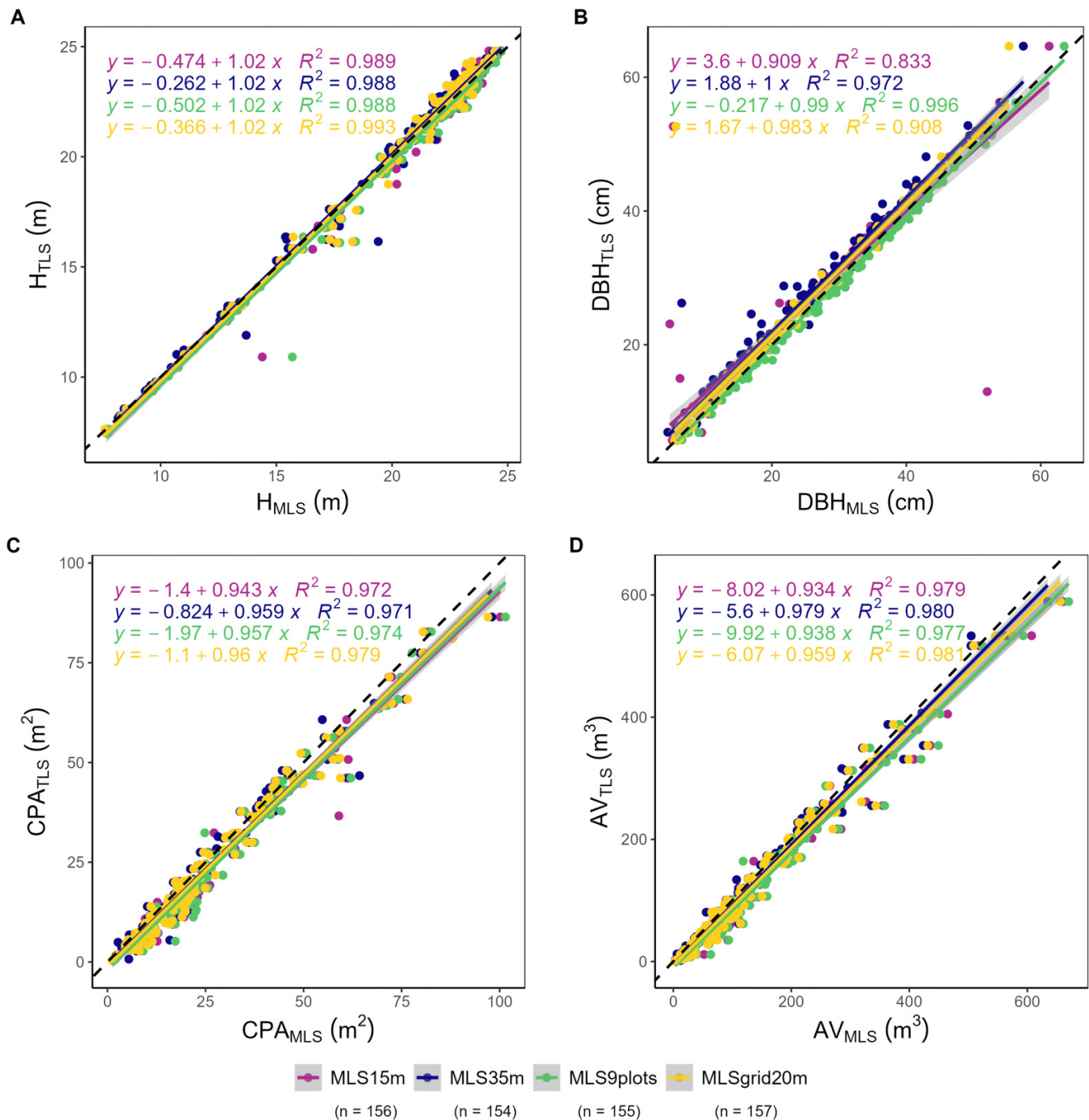
Accuracy of the estimated tree attributes was assessed by calculating the coefficient of determination (R²) (eq. 1), RMSE (eq. 2), the relative RMSE (%) (eq. 3), the bias (eq. 4), and the relative bias (%) (eq. 5):

$$(1) \quad R^2 = 1 - \frac{\sum_{i=1}^n (\hat{y}_i - y_i)^2}{\sum_{i=1}^n (\bar{y}_i - y_i)^2}$$

$$(2) \quad \text{RMSE} = \sqrt{\frac{1}{n} \sum_{i=1}^n (\hat{y}_i - y_i)^2}$$

$$(3) \quad \text{RMSE} (\%) = \frac{\text{RMSE}}{\text{mean}(\bar{y})} \times 100$$

Fig. 4. Regression analysis between tree attributes estimated from terrestrial laser scanning (TLS) (reference) and mobile laser scanning (MLS): (A) height (H), (B) diameter at breast height (DBH), (C) crown projected area (CPA) and (D) alpha volume (AV). Results are presented for four MLS acquisition scenarios: MLS_{15m} (purple), MLS_{35m} (blue), MLS_{9plots} (green), and MLS_{grid20m} (yellow). “n” denotes the number of trees that were identified through automated segmentation and matching against the 163 TLS reference trees, as detailed in Section 2.4.1. The dashed line represents the 1:1 line. The grey band is the 95% confidence band for predictions.



$$(4) \quad \text{bias} = \frac{1}{n} \sum_{i=1}^n (\hat{y}_i - y_i)$$

$$(5) \quad \text{bias} (\%) = \frac{\text{bias}}{\text{mean}(\hat{y})} \times 100$$

where n represents the number of trees, y_i is the reference TLS/field inventory attribute that was measured for the i -th tree, \hat{y}_i is the estimated attribute for the i -th tree that was derived from MLS data, and \bar{y}_i is the mean of the TLS/field inventory reference attribute.

Table 3. Estimation accuracy (root-mean square error (RMSE) and bias) of tree attributes for the four mobile laser scanning (MLS) acquisition scenarios: height (H), diameter at breast height (DBH), crown projected area (CPA) and alpha volume (AV).

Scenario	H (m)		DBH (cm)		CPA (m ²)		AV (m ³)	
	RMSE	bias	RMSE	bias	RMSE	bias	RMSE	bias
MLS _{15m}	0.50 (2.51%)	0.11 (0.55%)	5.35 (19.85%)	-1.25 (-4.64%)	4.43 (19.32%)	2.89 (12.60%)	25.96 (21.39%)	17.22 (14.19%)
MLS _{35m}	0.49 (2.44%)	-0.11 (-0.55%)	2.76 (10.18%)	-1.91 (-7.05%)	3.77 (16.39%)	1.84 (8.00%)	19.19 (15.75%)	8.28 (6.80%)
MLS _{9plots}	0.55 (2.77%)	0.20 (1.01%)	0.94 (3.54%)	0.50 (1.88%)	4.38 (19.51%)	3.08 (13.72%)	27.13 (22.86%)	18.39 (15.49%)
MLS _{grid20m}	0.41 (2.07%)	0.00 (0.00%)	3.98 (14.93%)	-1.25 (-4.69%)	3.51 (15.59%)	2.07 (9.19%)	20.91 (17.59%)	11.46 (9.64%)

3. Results

3.1. MLS versus TLS: H, DBH, CPA, and AV

Tree attributes that were estimated from TLS and MLS data exhibit strong similarities across all scenarios (Fig. 4). H_{MLS} , CPA_{MLS} , and AV_{MLS} demonstrated good agreement with TLS data, with RMSE values ranging from 2.07% to 2.77% (0.41 to 0.55 m), 15.59% to 19.51% (3.51 to 4.38 m²), and 15.75% to 22.86% (19.19 to 27.13 m³), respectively, across all scenarios (Table 3). DBH_{MLS} exhibits RMSE values ranging from 3.54% (MLS_{9plots}) to 19.85% (MLS_{15m}) (i.e., from 0.94 to 5.35 cm) (Fig. 4B). The bias remains below 5% in all scenarios (~1 cm), except for MLS_{35m}, which exhibits a bias of -7.05% (-1.91 cm) compared to TLS. Among the scenarios, the MLS_{grid20m} yielded the most favourable results, displaying low bias for all attributes (less than 10%). Overall, these results demonstrate the method's reliability in extracting tree attributes, showing high consistency across different scenarios.

3.2. MLS versus TLS: V_{tot} , V_{merch} , V_{op} , and V_{stem}

$V_{\text{tot_MLS}}$ was overestimated across the four MLS acquisition scenarios (Figs. 5A–5D), with RMSE values ranging from 22.9% (MLS_{35m}) to 46.77% (MLS_{9plots}) and bias ranging from 16.22% (MLS_{35m}) to 37.89% (MLS_{9plots}). A comparable tendency towards overestimation was observed in $V_{\text{merch_MLS}}$ (Figs. 5E–5H), especially for larger volumes (≥ 1.5 m³). The RMSE varied from 15.15% (MLS_{35m}) to 31.16% (MLS_{9plots}), with bias ranging from -5.87% (MLS_{35m}) to 20.83% (MLS_{9plots}). $V_{\text{op_MLS}}$ across the four MLS scenarios demonstrated high accuracy, exhibiting minor variations and a strong correlation with TLS data, as shown in Figs. 5I–5L. Yet, we observed a slight overestimation of $V_{\text{op_MLS}}$ across all scenarios, except for MLS_{35m}, which showed underestimation. The RMSE ranged from 14.6% (MLS_{grid20m}) to 22.32% (MLS_{9plots}), while bias ranged from 5.64% (MLS_{15m}) to 12.51% (MLS_{9plots}). $V_{\text{stem_MLS}}$ demonstrated the highest accuracy among the volume types assessed, with RMSE around 10% and negative biases <5% for both MLS_{9plots} and MLS_{grid20m} (Figs. 5O–5P). This slight underestimation was consistent across all scenarios but was more pronounced for MLS_{35m} (bias = -21.29%) and MLS_{15m} (bias = -9.93%). MLS_{35m} acquisition scenario was closely aligned with TLS data for $V_{\text{merch_MLS}}$ (Fig. 5F) and $V_{\text{op_MLS}}$ (Fig. 5J). Yet, a compensatory effect was observed for these results, marked by an underestimation of $V_{\text{stem_MLS}}$ (Fig. 5N) and an overestimation of $V_{\text{tot_MLS}}$ (Fig. 5B). Overall, the MLS_{grid20m}

scenario excelled for accurately estimating both $V_{\text{op_MLS}}$ and $V_{\text{stem_MLS}}$.

Figure 6 presents a breakdown of $V_{\text{merch_MLS}}$ by branching order, ranging from the first-level branches (order 1) to the third-level branches (order 3), comparing these estimates against the QSM-derived values from TLS data. The analysis reveals a consistent overestimation of each branching order from $V_{\text{merch_MLS}}$ across all scenarios, with the degree of overestimation intensifying for higher orders. While there is a strong correlation for branching order 1 between TLS and MLS estimations, substantial overestimations by MLS are evident for branching orders 2 and 3.

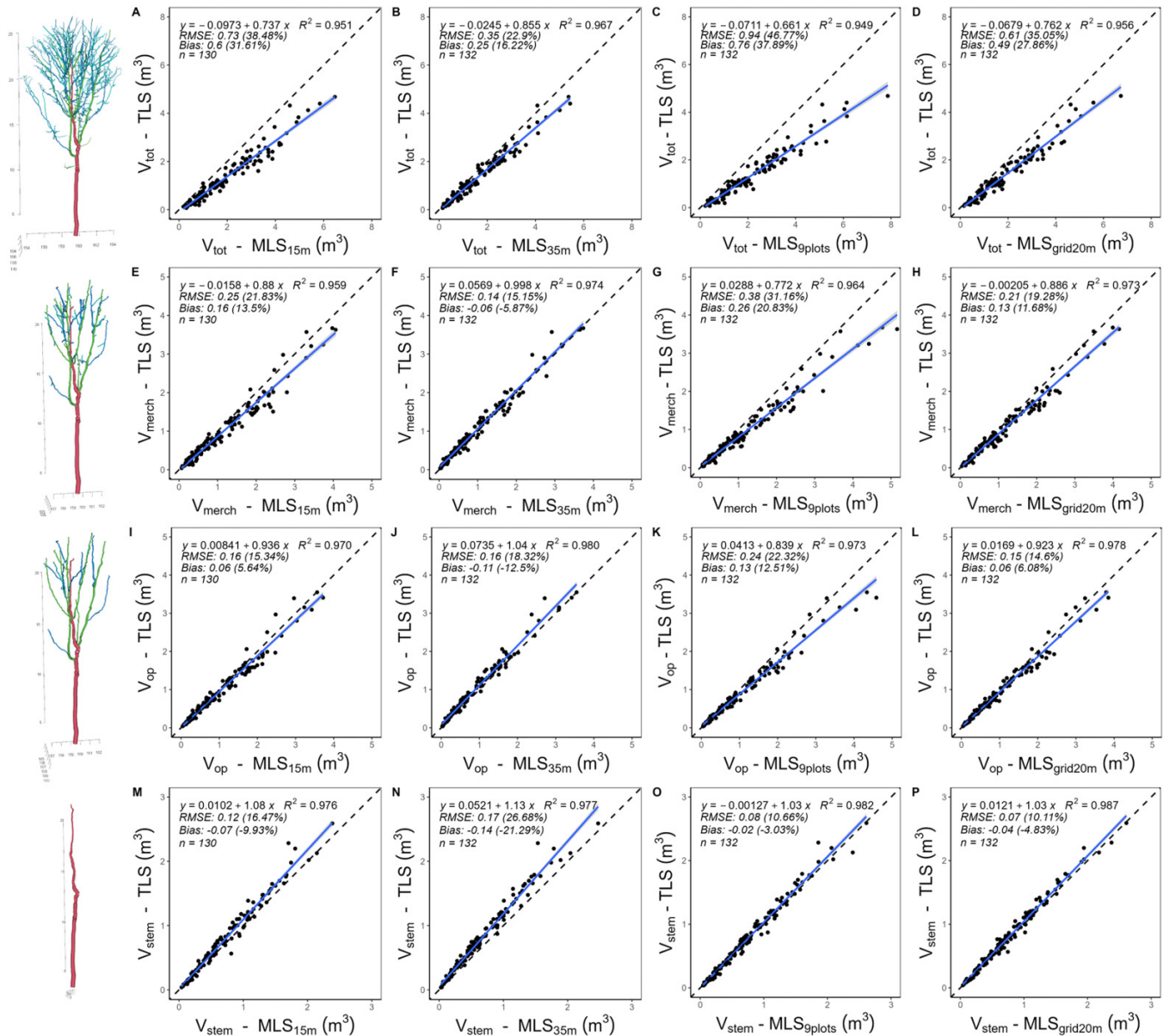
Among the different acquisition scenarios, the MLS_{35m} scenario exhibits the best results for branching order 1, with an RMSE of 50.81% and a bias of 12.28%. Similarly, the MLS_{grid20m} scenario performs well, with an RMSE of 51.93% and a bias of 34.04% for branching order 1. Nevertheless, it should be noted that similar trends were observed between the different acquisition scenarios.

3.3. MLS versus destructive sampling versus Taper model: V_{op} and V_{stem}

$V_{\text{op_MLS}}$ exhibits a trend towards overestimation across all scenarios when compared to destructive field measurements. This overestimation becomes more pronounced with increasing tree dimensions (Figs. 7A–7D). Conversely, smaller-sized trees ($V_{\text{op}} < 1.5$ m³) tend to be slightly underestimated. Among the different scenarios, the MLS_{35m} scenario demonstrated the smallest bias (1.46%) and RMSE (22.04%). Yet, it is worth noting that this scenario had the poorest model fit, as indicated by an R^2 value of 0.809. The MLS_{15m} and MLS_{grid20m} scenarios produced similar results for $V_{\text{op_MLS}}$, with biases of 13.26% and 14.01%, and RMSE values of 22.42% and 24.14%, respectively. In contrast, the MLS_{9plots} scenario showed the most significant overestimation, with a bias of 21.32% and an RMSE of 29.63%. Overall, results compared to destructive sampling display the same trends noted in the comparison with TLS data (Figs. 5I–5L).

$V_{\text{stem_MLS}}$ aligns closely with the outputs from the Li and Weiskittel regional taper model (Figs. 7E–7H). Consistency was maintained across scenarios, except for MLS_{35m}, which showed a slight underestimation of $V_{\text{stem_MLS}}$. This trend was also observed against TLS data (Fig. 5N). The MLS_{9plots} and MLS_{grid20m} scenarios showed low biases of 0.05% (Fig. 7G) and -1.44% (Fig. 7H), respectively, affirming the accuracy of MLS in estimating merchantable stem volumes.

Fig. 5. Regression analysis for merchantable trees (DBH ≥ 8 cm) comparing TLS and MLS across four MLS acquisition scenarios (MLS_{15m}, MLS_{35m}, MLS_{9plots}, and MLS_{grid20m}): (A–D) total volume (V_{tot}), (E–H) merchantable volume (V_{merch}), (I–L) operational merchantable volume (V_{op}), and (M–P) merchantable stem volume (V_{stem}). “ n ” indicates the number of merchantable trees that were analyzed. The dashed line represents the 1:1 line. The grey area identifies the 95% confidence band. Visual representations of each volume type from the QSM analysis are shown to the left of their corresponding result row. The detailed description of each volume type is provided in Table 2. DBH, diameter at breast height; TLS, terrestrial laser scanning; MLS, mobile laser scanning.



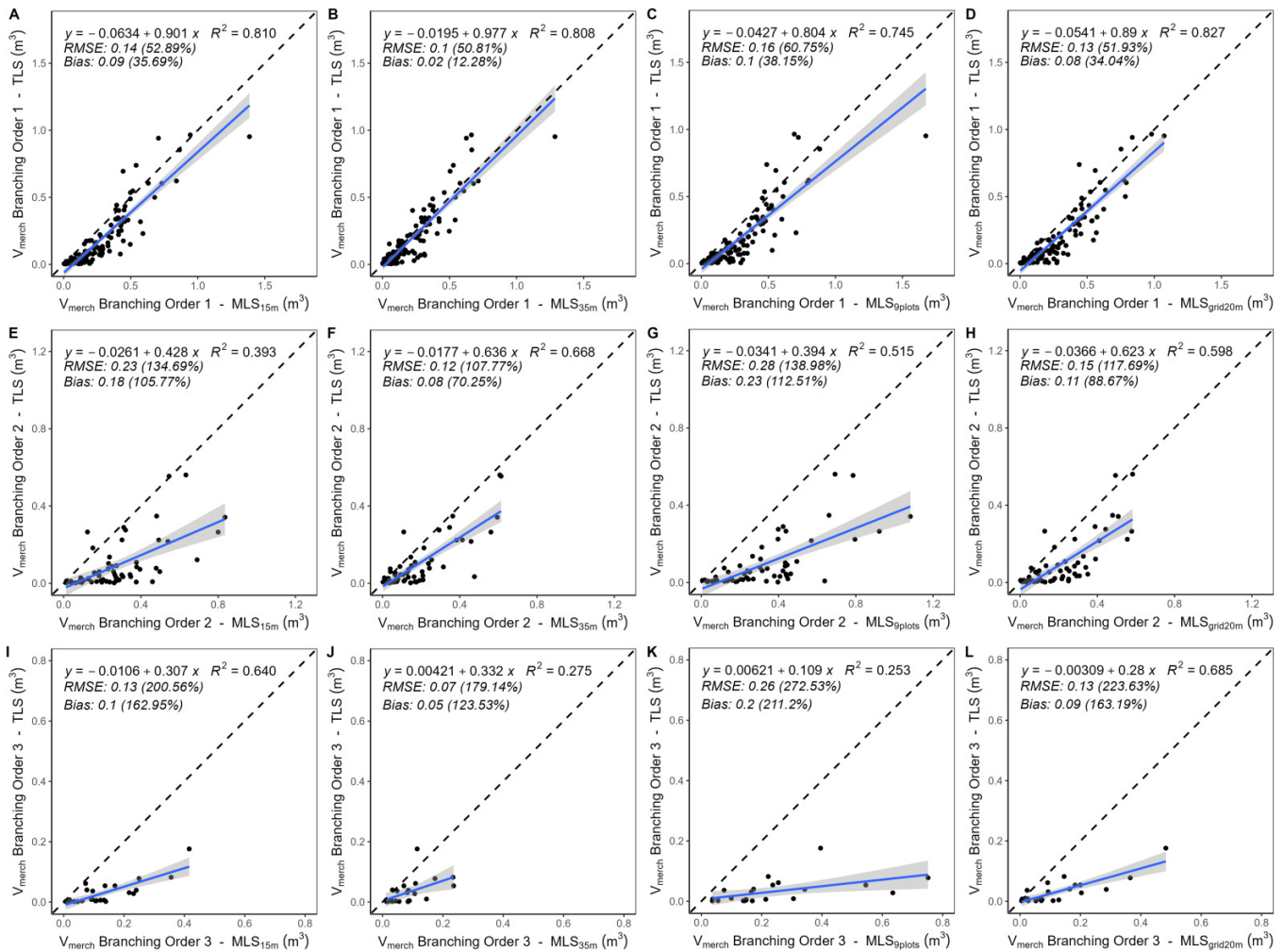
4. Discussion

4.1. Suitability of MLS for estimating tree attributes

The automated method to process MLS data for estimating tree structural attributes in a leaf-off temperate hardwood stand was accurate. H_{MLS} , CPA_{MLS} , and AV_{MLS} were in strong agreement with attributes from semi-automatically segmented TLS trees (Fig. 4 and Table 3). These results demonstrated the potential of automated segmentation and filter-

ing of MLS data in simple forest structures like mature hardwood stands (Fig. 1C). However, we noted a minor but systematic underestimation of DBH_{MLS} for most scenarios (Table 3). This slight underestimation is mainly due to the wider beam divergence of MLS compared to TLS, resulting in fuzzier representations of stem boundaries in the point clouds, which impacts the circle fitting algorithm. This effect, visible in Fig. 3, was also observed in studies by Bauwens et al. (2016), Kuželka et al. (2022), and Stovall et al. (2023). Improving DBH accuracy might involve creating filtering algorithms specif-

Fig. 6. Regression analysis of merchantable volume (V_{merch}) derived from TLS and MLS data decomposed by branching order: (A–D) order 1 = first-level branches; (E–H) order 2 = second-level branches; (I–L) order 3 = third-level branches. The results are presented for the four MLS acquisition scenarios (MLS_{15m}, MLS_{35m}, MLS_{9plots}, and MLS_{grid20m}). The dashed line represents the 1:1 line. The area in grey identifies the 95% confidence interval. The detailed description of V_{merch} is provided in Table 2. TLS, terrestrial laser scanning; MLS, mobile laser scanning.

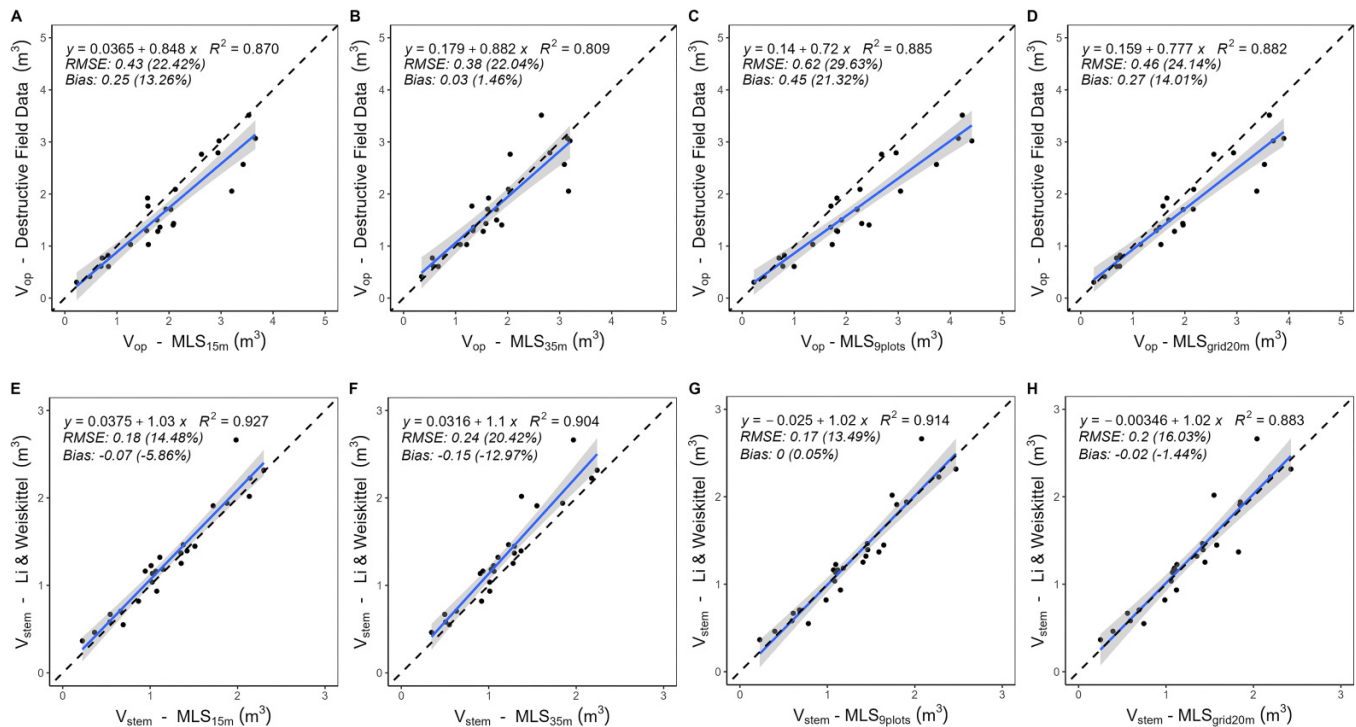


ically designed for MLS data, which would more effectively identify the stem’s surface and preserve adequate point density for the fitting process.

$V_{\text{stem_MLS}}$ was highly reliable, yet, similar to DBH, it showed a slight underestimation (negative bias < 10%) compared to TLS and Li and Weiskittel’s taper model in all scenarios except MLS_{35m}. This underestimation, similar to that noted by Chiappini et al. (2022) in a black pine plantation (bias = -4.1%; RMSE = 12.4%), likely arises from the QSM algorithm’s cylinder fitting process, which minimizes point-to-surface distance from noisier MLS point cloud, as evidenced in Fig. 8C. Stovall et al. (2023) attributed 60% of the MLS-based stem assessments uncertainty to laser beam divergence and point density, which showed positive and negative correlations, respectively. Their comparison of stem taper estimates from TLS and MLS against field measurements in the Harvard Forest revealed both lidar systems as nearly unbiased, yet stem taper error increased with height, with TLS offer-

ing more reliable diameter assessments (RMSE = 1.93 cm, 9.57%) than MLS (RMSE = 2.59 cm, 12.84%). López Serrano et al. (2022) also achieved nearly unbiased stem volume estimates in Spanish forests with a slight overestimation of 1.37% (RMSE = 14.3%) using handheld MLS, verified against 71 destructively sampled trees. To alleviate bias in the estimate, Hyyppä et al. (2020) introduced a post-SLAM algorithm filter using arc detection, which led to bias levels below 3% and RMSE under 10% for stem volume estimation in Finnish coniferous forests. Using a similar approach, Winberg et al. (2023) explored the use of MLS data for estimating log volume of 457 Norway spruce against X-ray data and observed a slight overestimation of the MLS-based estimate (bias of 0.024 m³ or 10.2%), which was mainly attributed to bark removal associated with the X-ray-based estimate. Overall, our results and those from other studies highlight the potential of MLS to accurately estimate stem volumes under diverse forest conditions, while emphasizing the need to adapt algorithms and

Fig. 7. (A–D) Regression analysis of operational merchantable volume (V_{op}) derived from destructive field measurements and MLS trees. (E–H) Regression analysis of merchantable stem volume (V_{stem}) that was derived from Li and Weiskittel’s taper model and MLS trees. The results are presented for the four MLS acquisition scenarios (MLS_{15m}, MLS_{35m}, MLS_{9plots}, and MLS_{grid20m}). $n = 26$ trees. The dashed line represents the 1:1 line. The area in grey identifies the 95% confidence interval. The detailed description of V_{op} and V_{stem} are provided in Table 2. MLS, mobile laser scanning.



methodologies to improve accuracy, particularly in handling noisier MLS point cloud data.

Our results also demonstrated that MLS overestimates branch volume with increasing bias with branching order (Fig. 6), indicating limitations of the MLS point cloud to depict fine-scale tree branch thickness. This resulted in an overestimation of V_{tot_MLS} , V_{merch_MLS} , and V_{op_MLS} in hardwood trees for all scenarios, except for MLS_{35m} (Fig. 5). Such overestimations in smaller tree parts along the stem have been previously reported (Winberg et al. 2023, Bornand et al. 2023). Notably, Abegg et al. (2023) observed amplified noise effects when scanning smaller objects, largely due to prevalent edge effects where a laser pulse intersects multiple objects, creating points off the object’s surface. We therefore attribute much of the branch overestimation in our study to the larger beam divergence of the MLS sensor (0.17°, yielding a 29.67 mm diameter laser beam at 10 m) compared to TLS (0.015°, yielding a 2.62 mm laser beam at 10 m), which amplifies these edge effects. This response is visually supported by Fig. 8D that shows MLS enlargement of branches leading to overestimated canopy branch volume in QSM calculations, which was also a trend that was identified by Demol et al. (2022b) and Vandendaele et al. (2022). Future research that is aimed at improving MLS-based branch volume assessments may benefit from the use of MLS sensors with lower beam divergences or from incorporating specialized noise-filtering techniques, such as heuristic denoising that was proposed by

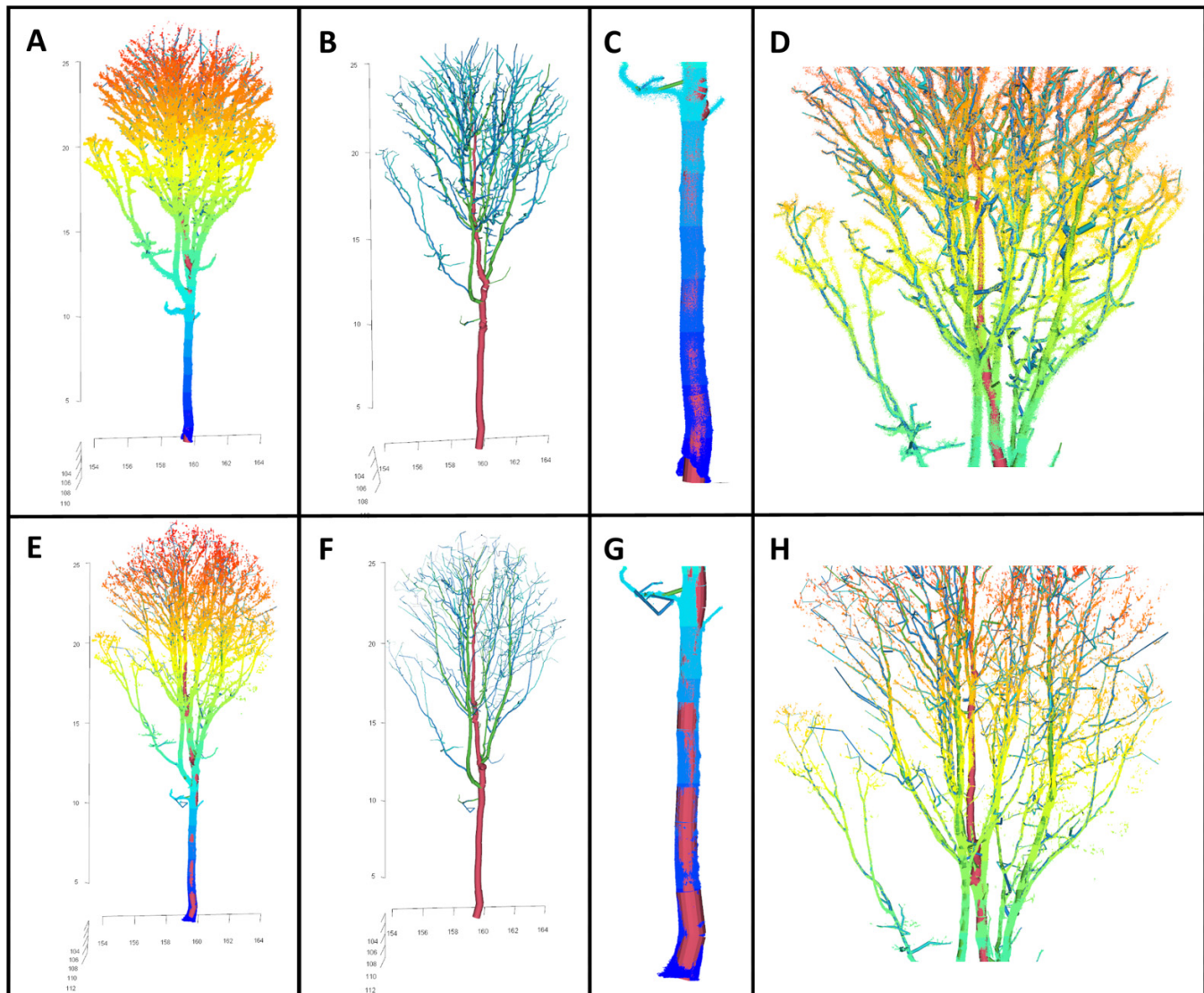
Winberg et al. (2023), intensity return filters (Kuzelka et al. 2022), or filters for altered shape pulses (Wilkes et al. 2017).

4.2. Influence of the acquisition scenario on tree attribute accuracy

Among the scenarios, MLS_{grid20m} yielded the best overall results, consistently showing low errors and bias for all attributes, thereby confirming its suitability for large-scale data collection and inventory. In contrast, the MLS_{35m} scenario, while being time-efficient (Fig. 2) and reliable for capturing crown attributes, significantly underestimated DBH_{MLS} and V_{stem_MLS} , thereby limiting its suitability for inventory purposes. For branch volume estimation, the MLS_{9plots} scenario showed the largest overestimation compared to TLS and destructive sampling, making it suboptimal for V_{tot_MLS} , V_{merch_MLS} , and V_{op_MLS} assessments. This trend was largely attributed to increased noise and oversampling due to the dense acquisition pattern, as discussed further below. The MLS_{15m} scenario was closely aligned with MLS_{grid20m}, but it showed slightly reduced accuracy, particularly in estimating DBH_{MLS} and V_{stem_MLS} , emphasizing the advantage of grid patterns for assessing tree attributes in MLS point clouds.

Previous studies on the effects of data acquisition on tree volume estimation have mainly used TLS, with limited or no interest to MLS acquisition patterns, particularly at the 1 ha scale. For instance, Wilkes et al. (2017) provided a compre-

Fig. 8. Illustration of the total volume (V_{tot}) of MLS (A–D) and TLS (E–H) tree extracted using *TreeQSM*: (A; E) 3 D point clouds and QSMs; (B; F) QSMs of the tree; (C; G) QSMs of the stem; (D; H) QSMs of the crown. The detailed description of V_{tot} is provided in [Table 2](#). TLS, terrestrial laser scanning; MLS, mobile laser scanning; QSM, quantitative structural models.

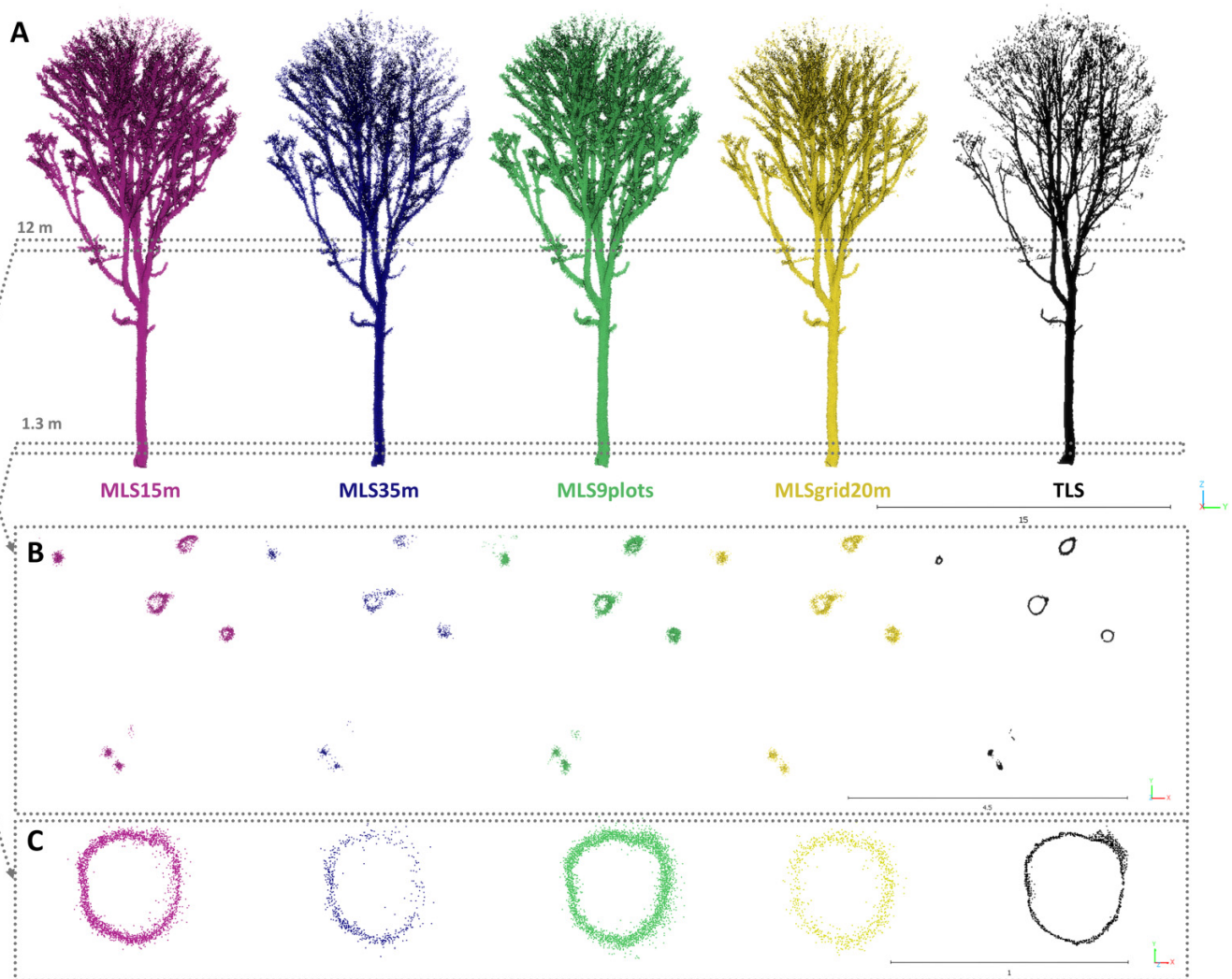


hensive review on multi-scan TLS sampling strategies for tree volume assessment on large forest plots (≥ 1 ha) and recommended a $10 \text{ m} \times 10 \text{ m}$ sampling grid pattern resulting in a 3–8 days of acquisition. Our study extends [Wilkes et al.'s \(2017\)](#) recommendations to MLS data, advocating for a similar grid pattern in large-scale data collections. A spacing of 20 m proved optimal in our simple forest structure, resulting in approximately 1 h of acquisition and 4 h of data preprocessing for a 1 ha site. The strength of the SLAM-based process lies in the simplicity of georeferencing, which facilitates large-scale data acquisition. While the MLS point cloud's noisier nature may reduce attribute estimation accuracy compared to TLS ([Figs. 5 and 8](#)), its flexibility and rapid data acquisition are an asset. Interestingly, the $V_{\text{op_MLS}}$ values from the $\text{MLS}_{\text{grid}20 \text{ m}}$ scenario ([Fig. 7D](#); $\text{RMSE} = 24.14\%$, $\text{bias} = 14.01\%$) closely matched those from [Bornand et al. \(2023\)](#) using a cost-effective Leica BLK360 TLS (Leica Geosystems, Heerbrugg,

Switzerland) ($\text{RMSE} = 25.68\%$; $\text{bias} = 14.16\%$), both benchmarked against destructive hardwood measurements. These results highlight the needs of further investigating the potential of MLS for wood volume assessment under a wide range of forest conditions.

Our study reveals that the $\text{MLS}_{15 \text{ m}}$ pattern, augmented with diagonal paths for better data coverage, also yields promising results for extracting tree structural attributes. In line with our results, [Tupinambá-Simões et al. \(2023\)](#) found that a parallel line acquisition pattern in a 1 ha mixed and irregular Mediterranean forest site increased tree detection compared to a cloverleaf trajectory, but did not significantly affect height and DBH accuracy. Similarly, [Kučelka et al. \(2022\)](#) in a Czech mixed wood forest noted that different MLS acquisition scenarios had minor impact on DBH estimate accuracy. They highlighted the advantage of rotary scan sensors like the GeoSLAM Zeb Horizon (GeoSLAM Ltd., Notting-

Fig. 9. Comparative visualization of an individual tree scanned from different MLS acquisition scenarios over the 1 ha study site against TLS data: (A) individual tree captured at the centre of the study site's leftmost plot (refer to Fig. 2) and automatically processed (Fig. 3), (B) cross-sectional view of 10 cm width from the lower part of the crown indicating merchantable branches, and (C) cross-section view of 10 cm width at DBH (1.3 m height), demonstrating point distribution and density. MLS, mobile laser scanning; TLS, terrestrial laser scanning; DBH, diameter at breast height.



ham, UK) or the Hovermap used in our study, which can capture a comprehensive scene every second, greatly reducing the influence of acquisition trajectory on point cloud quality unlike photogrammetry. These findings, along with ours, demonstrate the efficacy of MLS in estimating structural tree attributes across various forest types. They suggest that while the specific MLS data acquisition pattern may be less critical, factors such as scanner proximity to trees, time efficiency, and trajectory looping to minimize distortions and signal occlusion are paramount in planning a data acquisition scenario.

The findings from the MLS_{9plots} scenario, corroborated by Mokroš et al. (2021), indicate that overly dense or repetitive MLS acquisition patterns are likely to introduce additional noise into the data. Mokroš et al. (2021) used an intensive 5 m × 5 m grid pattern with GeoSLAM Zeb Horizon in forest of European beech (*Fagus sylvatica*) and Nor-

way spruce (*Picea abies*), where they observed significant noise and misalignment problems in MLS point clouds, resulting in notable DBH estimation errors (RMSE = 6.26 cm, bias = 4.34 cm). They attributed this effect to the dense acquisition pattern amplifying geometric discrepancies and SLAM alignment issues. While our study did not face misalignment problems or stem duplication, unlike Mokroš et al. (2021), the MLS_{9plots} scenario exhibited the highest occurrence of noise around stem bases, resulting in an integration of low vegetation and ground points following the tree segmentation step. Yet, this issue was effectively addressed by our tree-base cleaning filter (section 2.4.2) (Fig. 3). Furthermore, while the MLS_{9plots} scenario accurately characterized stems, it exhibited the most pronounced overestimation of branch volume, which could be mainly attributed to increased noise around branches (Fig. 9). In conformity with these observations, Abegg et al. (2023) observed that increasing the num-

Table 4. Time requirement for each step of the developed workflow apply on the nine sample plots (+10 m radius buffer) within the 1 ha study site.

Acquisition scenario	Time consumption						
	Data acquisition	Data preprocessing	Tree segmentation	Tree filtering	Tree attributes	QSM creation	QSM truncation
MLS _{15m}	30 min	3.5 h	30 min	8 min	2 h	2 days	30 min
MLS _{35m}	15 min	2 h	20 min	8 min	2 h	1.5 days	30 min
MLS _{9plots}	35 min	4 h	35 min	8 min	2 h	2 days	30 min
MLS _{grid20m}	40 min	4 h	45 min	8 min	2 h	2 days	30 min
TLS	6.5 h	6 h	50 min	8 min	2 h	2 days	30 min

Note: The processing was performed on a computer with a 12th Gen Intel(R) Core (TM) i9-12900—2.40 GHz processor, 128 GB RAM. MLS, mobile laser scanning; TLS, terrestrial laser scanning; QSM, quantitative structural models.

ber of TLS scanner positions not only improved the accuracy of merchantable wood volume estimates, but also introduced greater variability and slight overestimation in smaller branches, compared to single scans. This trend can be further intensified by wind conditions (Vaaja et al. 2016), highlighting the drawbacks of excessively dense or repetitive scanning acquisitions that can amplify such discrepancies. Overall, these results indicate that optimizing MLS data acquisition requires choosing patterns that favour uniform coverage from multiple viewpoints while minimizing oversampling and noise.

4.3. Limitations

The current method, although automated, requires multiple software tools (Computree, Matlab, and R), prompting the need for research to consolidate algorithms into one open-source environment like R or Python for efficiency and accessibility. As MLS technology becomes more user-friendly, it offers vast 3 D data potential for foresters. The main constraints are QSM computations (Table 4) that are time-consuming, and which limits their operational potential. Therefore, we strongly encourage researchers to prioritize the development of QSM algorithms that can offer faster processing capabilities and effectively handle a large number of trees.

Another study limitation is that TLS validation data (163 trees) are not entirely error-free, given that TLS is prone to occlusion, particularly at the crown level. This can lead to QSM underestimation (Fig. 8). Regarding the results, it can be hypothesized that overestimation of MLS branch volume is mainly influenced by three factors: (i) the wider MLS beam divergence; (ii) SLAM propagation errors; and (iii) a potential underestimation of TLS branch volume due to occlusion phenomena. Currently, TLS remains the most accurate technology and is widely recognized as the preferred validation tool (Calders et al. 2020; Duncanson et al. 2021). The strong correlation that was observed in our previous study between manual measurements of wood volume on felled trees with TLS-derived estimates further validates the use of TLS as a reference tool (Vandendaele et al. 2022). Yet, it is important for further studies, such as those conducted by Lau et al. (2018) and Demol et al. (2022b), to include manual measurements of the size of commercial branches to accurately quantify the bias that is observed with both TLS and MLS in relation to field reality. The panels within Fig. 6 indicate that it may be possible

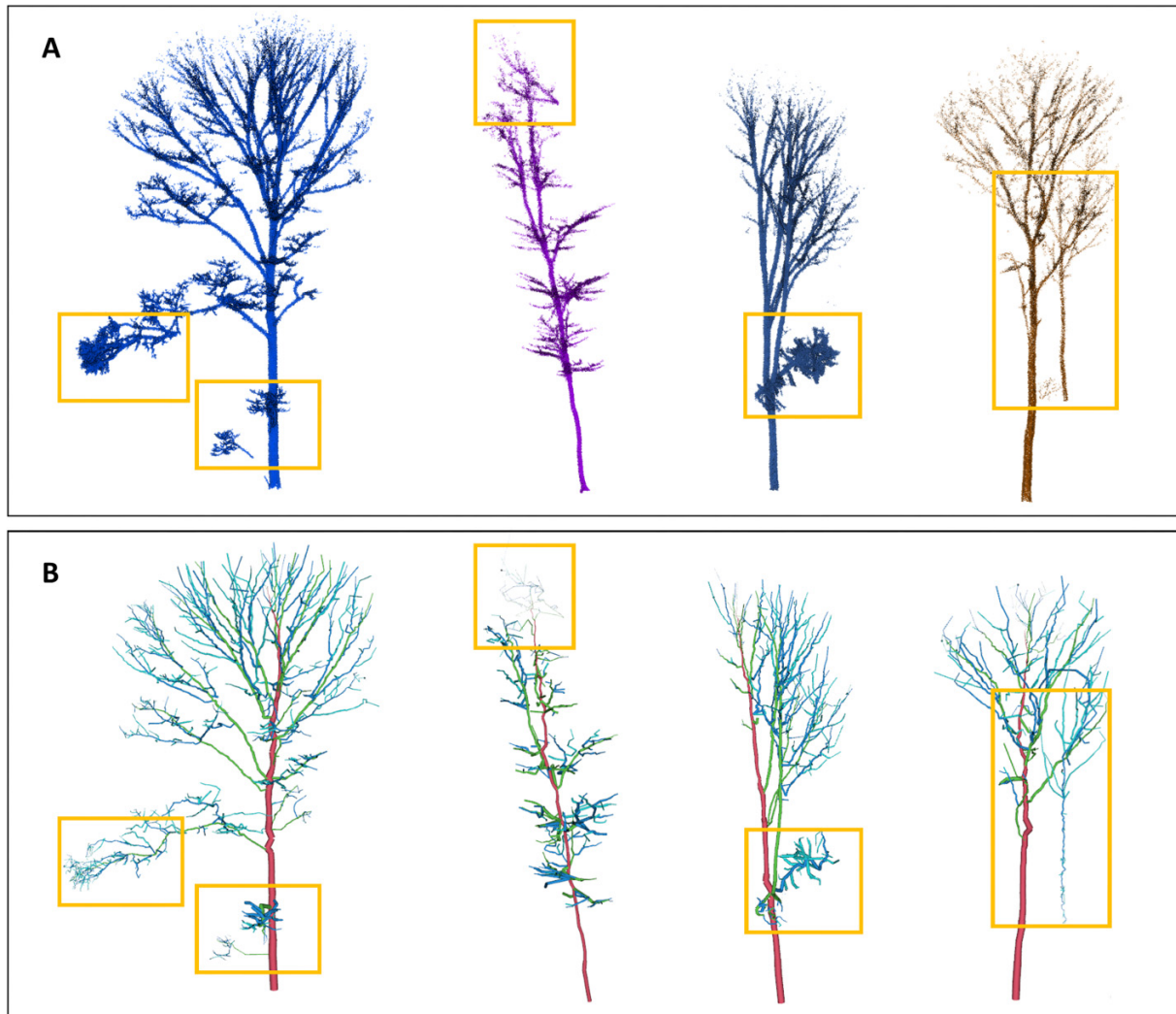
to develop a correction factor for the MLS-derived values, by branch order, to compensate for the overestimation of wood volume. This correction is likely to be derived from physical considerations of the size of the wood segment in relation to beam divergence and the operation distance to the target.

Importantly, while automation offers significant operational efficiency gains, it is not without potential errors, as depicted in Fig. 10. Our study was conducted in a mature hardwood forest with minimal undergrowth, flat terrain, and well-spaced trees. We found that segmentation errors were not prevalent; rather, there were isolated incidents (Figs. 4C–4D), confirming the overall effectiveness and robustness of the automated method across different acquisition scenarios. Yet, the application of automated processes and the impact of acquisition scenarios in more complex forest structures should be carefully evaluated, given that segmentation inaccuracies may result in large erroneous QSM outputs. For instance, in complex forests such as tropical ecosystems, Martin-Ducup et al. (2021) have shown that manual assistance in segmentation was essential to mitigate potential errors in volume estimates. Considering this, our next objective is to expand the scope of this study and assess the applicability of the developed method to a broader range of forest conditions, including structurally complex environments. By doing so, we aim to test the limits of MLS technology and enhance its understanding and usage.

4.4. Practical application for operational forestry

The study's findings on MLS systems in forest inventory have significant operational implications. MLS's efficiency in capturing detailed 3 D tree structural information has the potential to improve productivity and cost-effectiveness of inventory operations. Incorporating individual tree volumes from QSMs as reliable references could enhance or even substitute destructive measurements (Duncanson et al. 2021). Before MLS can be reliably used for tree volume and biomass estimation, significant challenges must be addressed. These include the detailed modeling of higher branching order architecture, the effective use of MLS in leaf-on forest conditions, and the integration of tree species and health conditions into the models. Recent advancements in deep learning hold promise for species prediction from 3 D point clouds (Seidel et al. 2021; Allen et al. 2022), although the process is

Fig. 10. (A) Segmented mobile laser scanning (MLS) point clouds of trees with insets (orange boxes) illustrating examples of segmentation errors. (B) Corresponding quantitative structural models (QSMs) derived from these point clouds with insets (orange boxes) indicating areas where segmentation inaccuracies have led to erroneous QSM structures.



still in early research stages. Increasing MLS data availability would likely drive further research on species identification, thereby enhancing allometric and biomass model development.

The significance of MLS technology becomes particularly pronounced when considering hardwood species, given that traditional destructive measurements can be laborious and allometric models often suffer from uncertainties, primarily due to the high variability in crown structure and proportion across species and along ontogeny. Building upon the potential of QSMs, it is important to evaluate how the accuracy of MLS-derived volumes reaches the acceptability thresholds that are used in forestry companies' yield tables. For hardwood species, the error margins that are identified for merchantable wood volume might exceed the acceptable threshold for forestry operations, which typically tolerate an error of 10%–20% from the actual tree volumes and aim for a bias-free estimate that does not exceed 5% (Fortin et al. 2007). Consequently, the error rates and bias that were observed in this

study for $V_{\text{merch_MLS}}$ may result in significant discrepancies in yield tables if they are used without correction.

Yet, the accuracy achieved for H_{MLS} , DBH_{MLS} , and $V_{\text{stem_MLS}}$ falls well within the operational acceptability range for operational use (Hyypä et al. 2020), particularly for the $\text{MLS}_{\text{grid}20\text{ m}}$ scenario. Our results suggest that with continuing refinement, MLS technology holds a significant potential for enhancing inventory applications. A substantial challenge in advancing MLS technology is the need to gather destructive ground truth data across diverse forest environments. This would help clarify the scope of observed errors and ensure they remain within the acceptable range of accuracy in estimating key inventory attributes.

5. Conclusion

This study demonstrates the significant potential of integrating QSM with MLS data as a non-destructive alternative to traditional sampling, promising advancements in the de-

velopment of allometric relationships for tree volume and biomass. Through the evaluation of various MLS data acquisition scenarios in a 1 ha mature leaf-off hardwood stand, we found that the MLS_{grid20 m} scenario achieved optimal results, indicating a low bias in key tree structural attributes when compared to TLS (i.e., bias < 5% for H, DBH, and V_{stem} and bias ~10% for CPA, AV, V_{op} , and V_{merch}). Yet, results from the MLS_{15 m} scenario were very close, suggesting that optimizing MLS data acquisition requires choosing acquisition patterns with uniform coverage, with paths close enough to minimize signal occlusion, while maintaining a distance between paths sufficiently large to minimize oversampling and noise.

Our method, employing automated segmentation and filtering of MLS point cloud, coupled with a QSM approach, resulted in accurate 3 D reconstruction of trees. The accuracy of stem volume estimations met the standards necessary for operational inventory purposes. However, branch volume estimations derived from MLS point clouds were prone to systematic overestimations, particularly noticeable in higher branching orders (2 and 3). Such overestimations compromise the accuracy needed for operational inventories, specifically in estimating merchantable and operational merchantable volumes. Addressing this issue may involve implementing a correction factor that accounts for the beam divergence of the MLS sensor and the specific scene configuration.

We can also assume that the MLS technology will improve rapidly. Future advances are most likely to occur in the refinement, adaptability, and automation of data processing methods at the plot or stand level. These advancements necessitate further testing of MLS-based methods across diverse forest ecosystems and the development of improved tree segmentation and filtering algorithms to accommodate complex forest structures. Additionally, optimizing QSM parameters for varied structural complexities remains a critical area for future research. Overall, this study highlights how MLS systems can contribute to enhancing forest inventory. The accuracy and efficiency of MLS data collection, combined with the ability to estimate tree attributes and merchantable wood volume, offer practical benefits for forest management.

Acknowledgements

We thank NHRI for providing the datasets used in this paper. We are particularly grateful to Pamela Hurley-Poitras for her extensive technical and logistical support throughout the study and for organizing and collecting the destructive measurements. We are also grateful to RMUS, our technical partners, for sharing their expertise on the use of the Hovermap MLS system. Special thanks to J.D. Irving Limited for allowing us to conduct this study in one of their hardwood stands and for felling and bucking the sampled trees. Thanks to W.F.J. Parsons for English language revision and to the reviewers for their valuable insights and contributions to this manuscript.

Article information

History dates

Received: 28 August 2023

Accepted: 12 February 2024

Accepted manuscript online: 26 February 2024

Version of record online: 8 May 2024

Copyright

© 2024 Copyright remains with the author(s) or their institution(s). This work is licensed under a [Creative Commons Attribution 4.0 International License](https://creativecommons.org/licenses/by/4.0/) (CC BY 4.0), which permits unrestricted use, distribution, and reproduction in any medium, provided the original author(s) and source are credited.

Data availability

The data that are presented in this study are available upon reasonable request from the corresponding author. The data are not publicly available because they were generated on private land and are subject to a confidentiality agreement with the landowner.

Author information

Author ORCIDs

Bastien Vandendaele <https://orcid.org/0000-0002-6142-9009>

Olivier Martin-Ducup <https://orcid.org/0000-0003-3795-1611>

Author notes

Richard A. Fournier served as Associate Editor at the time of manuscript review and acceptance and did not handle peer review and editorial decisions regarding this manuscript.

Author contributions

Conceptualization: BV, RAF, GP

Data curation: BV

Formal analysis: BV, OM

Funding acquisition: GP

Investigation: BV

Methodology: BV, OM

Project administration: BV, GP

Resources: GP

Software: BV, OM

Supervision: GP

Validation: BV, GP

Visualization: BV

Writing - original draft: BV

Writing - review & editing: BV, OM, RAF, GP

Competing interests

The authors declare no conflict of interest.

Funding information

This research was funded by private funds from the Northern Hardwoods Research Institute Inc. (NHRI), by Mitacs "Acceleration funding grant ref. FR60300," by NRCan CWFC FIP program and the New Brunswick Innovation Foundation.

References

- Abegg, M., Bösch, R., Kükenbrink, D., and Morsdorf, F. 2023. Tree volume estimation with terrestrial laser scanning—testing for bias in a 3D virtual environment. *Agric. For. Meteorol.* **331**. doi:[10.1016/j.agrformet.2023.109348](https://doi.org/10.1016/j.agrformet.2023.109348).

- Aguilar, F.J., Nemmaoui, A., Peñalver, A., Rivas, J.R., and Aguilar, M.A. 2019. Developing allometric equations for teak plantations located in the coastal region of Ecuador from terrestrial laser scanning data. *Forests*, **10**(12): 1050. doi:10.3390/F10121050.
- Åkerblom, M., Raunonen, P., Kaasalainen, M., and Casella, E. 2015. Analysis of geometric primitives in quantitative structure models of tree stems. *Remote Sens.* **7**(4): 4581–4603. doi:10.3390/rs70404581.
- Allen, M.J., Grieve, S.W.D., Owen, H.J.F., and Lines, E.R. 2022. Tree species classification from complex laser scanning data in Mediterranean forests using deep learning. *Methods Ecol. Evol.* **14**(7): 1657–1667. doi:10.1111/2041-210X.13981.
- Balenović, I., Liang, X., Jurjević, L., Hyyppä, J., Seletković, A., and Kukko, A. 2020. Hand-held personal laser scanning—current status and perspectives for forest inventory application. *Croat. J. For. Eng.* **42**(1): 165–183. doi:10.5552/crojfe.2021.858.
- Bauwens, S., Bartholomeus, H., Calders, K., and Lejeune, P. 2016. Forest inventory with terrestrial LiDAR: A comparison of static and hand-held mobile laser scanning. *Forests*, **7**(6): 127. doi:10.3390/f7060127.
- Bienert, A., Hess, C., Maas, H.G., and von Oheimb, G. 2014. A voxel-based technique to estimate the volume of trees from terrestrial laser scanner data. *Int. Arch. Photogramm. Remote Sens.* **XL-5**: 101–106. doi:10.5194/isprsarchives-XL-5-101-2014.
- Bornand, A., Rehush, N., Morsdorf, F., Thürig, E., and Abegg, M. 2023. Individual tree volume estimation with terrestrial laser scanning: evaluating reconstructive and allometric approaches. *Agric. For. Meteorol.* **341**. doi:10.1016/j.agrformet.2023.109654.
- Brede, B., Calders, K., Lau, A., Raunonen, P., Bartholomeus, H.M., Herold, M., and Kooistra, L. 2019. Non-destructive tree volume estimation through quantitative structure modelling: comparing UAV laser scanning with terrestrial LiDAR. *Remote Sens. Environ.* **233**: 111135. doi:10.1016/j.rse.2019.111355.
- Bruce, D., and Schumacher, F.X. 1950. *Forest Mensuration*, McGraw-Hill, New York, NY.
- Burt, A., Boni Vicari, M., Da Costa, A.C.L., Coughlin, I., Meir, P., Rowland, L., and Disney, M. 2021. New insights into large tropical tree mass and structure from direct harvest and terrestrial lidar. *R. Soc. Open Sci.* **8**(2). doi:10.1098/rsos.201458.
- Calders, K., Adams, J., Armston, J., Bartholomeus, H., Bauwens, S., Bentley, L.P., et al. 2020. Terrestrial laser scanning in forest ecology: expanding the horizon. *Remote Sens. Environ.* **251**. doi:10.1016/j.rse.2020.112102.
- Calders, K., Newnham, G., Burt, A., Murphy, S., Raunonen, P., Herold, M., et al. 2015. Nondestructive estimates of above-ground biomass using terrestrial laser scanning. *Methods Ecol. Evol.* **6**(2): 198–208. doi:10.1111/2041-210X.12301.
- Chave, J., Réjou-Méchain, M., Búrquez, A., Chidumayo, E., Colgan, M.S., Delitti, W.B.C., et al. 2014. Improved allometric models to estimate the aboveground biomass of tropical trees. *Global Change Biol.* **20**(10): 3177–3190. doi:10.1111/gcb.12629.
- Chen, S., Liu, H., Feng, Z., Shen, C., and Chen, P. 2019. Applicability of personal laser scanning in forestry inventory. *PLoS ONE*, **14**(2). doi:10.1371/journal.pone.0211392.
- Chiappini, S., Pierdicca, R., Malandra, F., Tonelli, E., Malinverni, E.S., Urbinati, C., and Vitali, A. 2022. Comparing Mobile laser scanner and manual measurements for dendrometric variables estimation in a black pine (*Pinus nigra* Arn.) plantation. *Comput. Electron. Agric.* **198**. doi:10.1016/j.compag.2022.107069.
- CloudCompare (version 2.11.3) [GPL software]. 2020. Available from <http://www.cloudcompare.org/> [accessed 20 December 2021].
- Demol, M., Verbeeck, H., Gielen, B., Armston, J., Burt, A., Disney, M., et al. 2022a. Estimating forest above-ground biomass with terrestrial laser scanning: current status and future directions. *Methods Ecol. Evol.* **13**(8): 1628–1639. doi:10.1111/2041-210X.13906.
- Demol, M., Wilkes, P., Raunonen, P., Moorthy, S.M.K., Calders, K., Gielen, B., and Verbeeck, H. 2022b. Volumetric overestimation of small branches in 3D reconstructions of *Fraxinus excelsior*. *Silva Fennica*, **56**. doi:10.14214/sf.10550.
- Duncanson, L., Armston, J., Disney, M., Avitabile, V., Barbier, N., Calders, K., et al. 2019. The importance of consistent global forest above-ground biomass product validation. *Surv. Geophys.* **40**: 979–999. doi:10.1007/s10712-019-09538-8.
- Duncanson, L., Disney, M., Armston, J., Nickeson, J., Minor, D., and Camacho, F. 2021. Aboveground woody biomass product validation good practices protocol. Version 1.0. doi:10.5067/doc/ceoswgcv/lpv/agb.001.
- Duncanson, L., Huang, W., Johnson, K., Swatantran, A., McRoberts, R.E., and Dubayah, R. 2017. Implications of allometric model selection for county-level biomass mapping. *Carbon Balance Manage.* **12**(1). doi:10.1186/s13021-017-0086-9.
- Fan, G., Xu, Z., Wang, J., Nan, L., Xiao, H., Xin, Z., and Chen, F. 2022. Plot-level reconstruction of 3D tree models for aboveground biomass estimation. *Ecol. Indic.* **142**. doi:10.1016/j.ecolind.2022.109211.
- Fortin, M., Deblois, J., Bernier, S., and Blais, G. 2007. Mise au point d'un tarif de cubage général pour les forêts québécoises: une approche pour mieux évaluer l'incertitude associée aux prévisions. *For. Chron.* **83**(5). doi:10.5558/tfc83754-5.
- Gollob, C., Ritter, T., and Nothdurft, A. 2020. Forest inventory with long range and high-speed personal laser scanning (PLS) and simultaneous localization and mapping (SLAM) technology. *Remote Sens.* **12**(9). doi:10.3390/RS12091509.
- Hackel, T., Wegner, J.D., and Schindler, K. 2016. Fast semantic segmentation of 3D point clouds with strongly varying density. *ISPRS Ann. Photogramm. Remote Sens. Spat., III-3*: 177–184. doi:10.5194/isprsannals-iii-3-177-2016.
- Hackenberg, J., Spiecker, H., Calders, K., Disney, M., and Raunonen, P. 2015. SimpleTree—an efficient open source tool to build tree models from TLS clouds. *Forests*, **6**(11): 4245–4294. doi:10.3390/f6114245.
- Hyyppä, E., Kukko, A., Kajaluoto, R., White, J.C., Wulder, M.A., Pyörälä, J., et al. 2020. Accurate derivation of stem curve and volume using backpack mobile laser scanning. *ISPRS J. Photogramm. Remote Sens.* **161**: 246–262. doi:10.1016/j.isprsjprs.2020.01.018.
- Jurjević, L., Liang, X., Gašparović, M., and Balenović, I. 2020. Is field-measured tree height as reliable as believed—Part II, A comparison study of tree height estimates from conventional field measurement and low-cost close-range remote sensing in a deciduous forest. *ISPRS J Photogramm Remote Sens.* **169**: 227–241. doi:10.1016/j.isprsjprs.2020.09.014.
- Kunz, M., Hess, C., Raunonen, P., Bienert, A., Hackenberg, J., Maas, H.G., et al. 2017. Comparison of wood volume estimates of young trees from terrestrial laser scan data. *iForest*, **10**(2): 451–458. doi:10.3832/ifer2151-010.
- Kuželka, K., Marušák, R., and Surový, P. 2022. Inventory of close-to-nature forest stands using terrestrial mobile laser scanning. *Int. J. Appl. Earth Obs. Geoinf.* **115**. doi:10.1016/j.jag.2022.103104.
- Lafarge, T., and Pateiro-Lopez, B. 2023. Package “alphashape3d” implementation of the 3D alpha-shape for the reconstruction of 3D sets from a point cloud. pp. 1–11. Available from <https://cran.r-project.org/web/packages/alphashape3d/index.html> [accessed 20 February 2021].
- Lau, A., Bentley, L.P., Martius, C., Shenkin, A., Bartholomeus, H., Raunonen, P., et al. 2018. Quantifying branch architecture of tropical trees using terrestrial LiDAR and 3D modelling. *Trees—Struct. Funct.* **32**(5): 1219–1231. doi:10.1007/s00468-018-1704-1.
- Lecigne, B. 2022. Package VoxR—Tree Geometry and Morphology from Unstructured TLS Data. *Ann. Bot.* **121**(4): 1–23. Available from <https://cran.r-project.org/web/packages/VoxR/index.html>.
- Lecigne, B., Delagrangé, S., and Messier, C. 2018. Exploring trees in three dimensions: VoxR, a novel voxel-based R package dedicated to analysing the complex arrangement of tree crowns. *Ann. Bot.* **121**(4): 589–601. doi:10.1093/aob/mcx095.
- Li, R., Weiskittel, A., Dick, A.R., Kershaw, J.A., and Seymour, R.S. 2012. Regional stem taper equations for eleven conifer species in the Acadian region of North America: development and assessment. *Northern J. Appl. For.* **29**(1): 5–14. doi:10.5849/njaf.10-037.
- Lin, L.I.-K. 1989. A concordance correlation coefficient to evaluate reproducibility. *Biometrics*, **45**(1): 255. doi:10.2307/2532051.
- López Serrano, F.R., Rubio, E., García Morote, F.A., Andrés Abellán, M., Picazo Córdoba, M.I., García Saucedo, F., et al. 2022. Artificial intelligence-based software (AID-FOREST) for tree detection: a new framework for fast and accurate forest inventory using LiDAR point clouds. *Int. J. Appl. Earth Obs. Geoinf.* **113**. doi:10.1016/j.jag.2022.103014.
- Martin-Ducup, O., and Lecigne, B. 2022. Package aRchi—quantitative structural model (QSM) Treatment for Tree Architecture. pp. 1–46. Available from <https://cran.r-project.org/src/contrib/Archive/aRchi/>.

- Martin-Ducup, O., Mofack, G., Wang, D., Raunonen, P., Ploton, P., Sonké, B., et al. 2021. Evaluation of automated pipelines for tree and plot metric estimation from TLS data in tropical forest areas. *Ann. Bot.* **128**(6): 753–766. doi:[10.1093/aob/mcab051](https://doi.org/10.1093/aob/mcab051).
- Mokroš, M., Mikita, T., Singh, A., Tomaščík, J., Chudá, J., Wężyk, P., et al. 2021. Novel low-cost mobile mapping systems for forest inventories as terrestrial laser scanning alternatives. *Int. J. Appl. Earth Obs. Geoinf.* **104**. doi:[10.1016/j.jag.2021.102512](https://doi.org/10.1016/j.jag.2021.102512).
- Momo Takoudjou, S., Ploton, P., Sonké, B., Hackenberg, J., Griffon, S., de Coligny, F., et al. 2018. Using terrestrial laser scanning data to estimate large tropical trees biomass and calibrate allometric models: A comparison with traditional destructive approach. *Methods Ecol. Evol.* **9**(4): 905–916. doi:[10.1111/2041-210X.12933](https://doi.org/10.1111/2041-210X.12933).
- Othmani, A., Piboule, A., Krebs, M., Stolz, C., and Yan Voon, L. 2011. Towards automated and operational forest inventories with T-Lidar. Available from <https://hal.archives-ouvertes.fr/hal-00646403> [accessed 15 January 2021].
- Perugia, B., Del, Giannetti, F., Chirici, G., and Travaglini, D. 2019. Influence of scan density on the estimation of single-tree attributes by hand-held mobile laser scanning. *Forests*, **10**(3). doi:[10.3390/f10030277](https://doi.org/10.3390/f10030277).
- R Core Team. 2017. R: a language and environment for statistical computing. R Foundation for Statistical Computing, Vienna, Austria. Available from <https://www.R-project.org/> [accessed 20 December 2021].
- Raunonen, P., and Åkerblom, M. 2019. InverseTampere/TreeQSM. Version 2.3.3. Available from <https://github.com/InverseTampere> [accessed 15 April 2021].
- Raunonen, P., Kaasalainen, M., Markku, Å., Kaasalainen, S., Kaartinen, H., Vastaranta, M., et al. 2013. Fast automatic precision tree models from terrestrial laser scanner data. *Remote Sens.* **5**(2): 491–520. doi:[10.3390/rs5020491](https://doi.org/10.3390/rs5020491).
- Seidel, D., Annighöfer, P., Thielman, A., Seifert, Q.E., Thauer, J.H., Glatthorn, J., et al. 2021. Predicting tree species from 3D laser scanning point clouds using deep learning. *Front. Plant Sci.* **12**. doi:[10.3389/fpls.2021.635440](https://doi.org/10.3389/fpls.2021.635440).
- Stovall, A.E.L., MacFarlane, D.W., Crawford, D., Jovanovic, T., Frank, J., and Brack, C. 2023. Comparing mobile and terrestrial laser scanning for measuring and modelling tree stem taper. *Forestry*, **96**(5): 705–717. doi:[10.1093/forestry/cpad012](https://doi.org/10.1093/forestry/cpad012).
- Terry, L., Calders, K., Åkerblom, M., Bartholomeus, H., Disney, M., Levick, S., et al. 2023. Analysing individual 3D tree structure using the R package ITSM. *Methods Ecol. Evol.* **14**(1): 231–241. doi:[10.1111/2041-210X.14026](https://doi.org/10.1111/2041-210X.14026).
- Tupinambá-Simões, F., Pascual, A., Guerra-Hernández, J., Ordóñez, C., de Conto, T., and Bravo, F. 2023. Assessing the performance of a hand-held laser scanning system for individual tree mapping—a mixed forests showcase in Spain. *Remote Sens.* **15**(5): 1169. doi:[10.3390/rs15051169](https://doi.org/10.3390/rs15051169).
- Vaaja, M.T., Virtanen, J.-P., Kurkela, M., Lehtola, V., Hyyppä, J., and Hyyppä, H. 2016. The effect of wind on tree stem parameter estimation using terrestrial laser scanning. *ISPRS Ann. Photogramm. Remote Sens. Spat. III-8*: 117–122. doi:[10.5194/isprsannals-iii-8-117-2016](https://doi.org/10.5194/isprsannals-iii-8-117-2016).
- Vandendaele, B., Martin-Ducup, O., Fournier, R.A., Pelletier, G., and Lejeune, P. 2022. Mobile laser scanning for estimating tree structural attributes in a temperate hardwood forest. *Remote Sens.* **14**(18). doi:[10.3390/rs14184522](https://doi.org/10.3390/rs14184522).
- Weiskittel, A., and Li, R. 2012. Development of regional taper and volume equations: hardwood species. Dendrometrics, LLC, Welches, OR.
- Wilkes, P., Lau, A., Disney, M., Calders, K., Burt, A., Gonzalez de Tanago, J., et al. 2017. Data acquisition considerations for terrestrial laser scanning of forest plots. *Remote Sens. Environ.* **196**: 140–153. doi:[10.1016/j.rse.2017.04.030](https://doi.org/10.1016/j.rse.2017.04.030).
- Winberg, O., Pyörälä, J., Yu, X., Kaartinen, H., Kukko, A., Holopainen, M., et al. 2023. Branch information extraction from Norway spruce using handheld laser scanning point clouds in Nordic forests. *ISPRS J. Photogramm. Remote Sens.* **9**: 100040. doi:[10.1016/j.isprsjprs.2023.100040](https://doi.org/10.1016/j.isprsjprs.2023.100040).
- Zelazny V.F. (ed.), and Ecosystem Classification Working Group. 2007. New Brunswick. Our landscape heritage: the story of ecological land classification in New Brunswick (2nd ed)/Notre patrimoine du paysage, l'histoire de la classification écologique des terres au Nouveau-Brunswick. Department of Natural Resources, Province of New Brunswick (NB), Canada.